Bridging the temperature and pressure gaps: close-packed transition metal surfaces in an oxygen environment

2008 J. Phys.: Condens. Matter 20 184021

(http://iopscience.iop.org/0953-8984/20/18/184021)

IOP Publishing Journal of Physics: Condensed Matter

J. Phys.: Condens. Matter **20** (2008) 184021 (19pp) doi:10.1088/0953-8984/20/18/184021

Bridging the temperature and pressure gaps: close-packed transition metal surfaces in an oxygen environment

Catherine Stampfl[1], Aloysius Soon[1], Simone Piccinin[1], Hongqing Shi[1] and Hong Zhang[1,2]

[1] School of Physics, The University of Sydney, Sydney New South Wales 2006, Australia
[2] School of Physical Sciences and Technology, Sichuan University, Chengdu 610065, People's Republic of China

E-mail: stampfl@physics.usyd.edu.au

Received 31 October 2007, in final form 11 February 2008
Published 17 April 2008
Online at stacks.iop.org/JPhysCM/20/184021

Abstract

An understanding of the interaction of atoms and molecules with solid surfaces on the microscopic level is of crucial importance to many, if not most, modern high-tech materials applications. Obtaining such accurate, quantitative information has traditionally been the realm of surface science experiments, carried out under ultra-high vacuum conditions. Over recent years scientists have realized the importance of obtaining such knowledge also under the high pressure and temperature conditions under which many industrial processes take place, e.g. heterogeneous catalysis, since the material under these conditions may be quite different to that under the conditions of typical surface science experiments. Theoretical studies too have been aimed at bridging the so-called pressure and temperature gaps, and great strides have been made in recent years, often in conjunction with experiment. Here we review recent progress in the understanding of the hexagonal close-packed surfaces of late transition and noble metals in an oxygen environment, which is of relevance to many heterogeneous catalytic reactions. In many cases it is found that, on exposure to high oxygen pressures and elevated temperatures, thin oxide-like structures form which may or may not be stable, and which may have little similarity to the bulk oxides, and thus possess unique chemical and physical properties.

(Some figures in this article are in colour only in the electronic version)

1. Introduction

The interaction of atoms and molecules with surfaces, and the chemical processes which occur thereon, play a critical role in the manufacture and performance of advanced materials which are used in high-tech applications, for example, electronic, magnetic, and optical devices, chemical sensors, heterogeneous catalysts, and hard and corrosion resistant coatings, to name a but few. In particular, the interaction of oxygen with transition metals (TMs) is of high importance for heterogeneous oxidation (and partial oxidation) catalysis (see e.g. [1–3]) and this has motivated large numbers of early studies on oxygen–metal interactions [4–6]. Extending atomic level understanding to elevated temperatures and pressures is highly desirable, and crucial to understanding the function of materials that occur under such conditions, but achieving such knowledge is often not straightforward. For many heterogeneous catalytic reactions, for example, it is now established that the characteristics of a material observed under ultra-high vacuum (UHV) conditions, where classical surface science techniques dominate, can be expected to be different to that under the high temperature and pressure conditions of technical catalysis. In this regime, it is much more problematic to obtain the same level of microscopic information. Nevertheless, there remains a general consensus that the clean metal surface, often assumed to be the catalyst, may not be the active material phase under such conditions.

Recently, through experimental and theoretical studies aimed at bridging such gaps, many interesting and significant findings have been reported; e.g., for the carbon monoxide

oxidation reaction over Ru(0001) and Pt(110), oxide patches on the surface exist which may be the active centers, in contrast to the hitherto believed pure metal. Furthermore, for TMs in an oxidizing atmosphere, formation of two-dimensional surface oxides, which may or may not bear a resemblance to the corresponding bulk oxides, has been discussed and identified [7, 8]. Such structures may possess unique properties and functionalities that are distinct to the related bulk phases. The formation and identification of thin surface oxidic structures on TMs has recently been reviewed; see, e.g., [9]. (See also the contribution by Seriani and Mittendorfer in the present issue.) These studies highlight the complex nature of the surface atomic structures that can form for oxygen/TM systems, and how they depend sensitively upon the 'environment', i.e. the gas pressure and temperature. The noble metals (Ag, Cu, and Au) are also important catalysts (see e.g. [10–12]), particularly for partial oxidation reactions. That Ag and Au are efficient catalysts is somewhat counterintuitive, since they bind oxygen and other adparticles only weakly. It is generally understood from Sabatier's principle [13] that a good catalyst should yield reaction intermediates that have an 'intermediate' or 'moderate' adsorption energy. In this way, the reactants will be stable under the pressure and temperature conditions of catalysis, but not so strongly bound that reaction is inhibited. The presence of thin oxide-like structures, or under-coordinated metal atoms which bind adspecies more strongly, has been put forward as possibly playing a role in certain catalytic reactions over these noble metals.

In the present paper, we review the theoretical work done over recent years, addressing the interaction of oxygen with hexagonal close-packed transition and noble metals. These studies are based on density-functional theory and employ the concept of *ab initio* atomistic thermodynamics to take into account the effects of temperature and pressure. This approach is described in section 2. In section 3 we begin by discussing the O/TM systems, starting with O/Ru(0001), which was one of the first to attract significant attention of theoretical and experimental studies, aimed at elucidating the active O species for the CO oxidation reaction. This is followed by the TMs to the right of ruthenium in the periodic table, which bind oxygen increasingly more weakly (i.e. Rh and Pd). The O/Ir(111) system is also discussed, where analogy to O/Rh(111) is made. In section 4, we discuss results for the interaction of oxygen with the 'coinage' (noble) metals, Cu, Ag, and Au, including a recent study on the interaction of oxygen with the Cu–Ag alloy. From all these results, various trends emerge, which are discussed in section 5.

2. *Ab initio* atomistic thermodynamics

The approach of *ab initio* atomistic thermodynamics applies to systems in equilibrium. It uses the results of first-principles calculations such as binding energies or surface energies, i.e. the information on the potential energy surface, to calculate appropriate thermodynamic potential functions like the Gibbs free energy [14–21]. With this approach, various structures are considered where it can be determined which is most stable for which values of the atom chemical potentials. For gas phase species, the chemical potential can be translated into pressure and temperature conditions. It is an indirect approach in the sense that its reliability is restricted to the structural configurations that are explicitly considered in the first-principles calculations. It is, nevertheless, very useful for a first understanding of a system, and initial identification of plausible, potentially important structures.

Considering a metal surface in contact with a gas phase of oxygen, the change in Gibbs free energy is calculated as

$$\Delta G(\mu_{\mathrm{O}}) = -\frac{1}{A}\left(G_{\mathrm{O/Surf}} - G_{\mathrm{Surf}} - N_{\mathrm{O}}\mu_{\mathrm{O}} - \Delta N_{\mathrm{M}}\mu_{\mathrm{M}}\right), \tag{1}$$

where $G_{\mathrm{O/Surf}}$ and G_{Surf} are the Gibbs free energies of the oxygen/TM system and clean surface, respectively. μ_{O} and μ_{M} are the atom chemical potentials of the oxygen and metal atoms, and N_{O} is the number of oxygen atoms contained in the surface structure. ΔN_{M} is the *difference* in the number of metal atoms between the O/TM system and the clean surface. The change in Gibbs free energy is normalized by the surface area A to allow comparisons between structures with different unit cells. We will refer to this quantity as 'change in Gibbs surface free energy of adsorption'. The chemical potential of the metal atom is taken to be that of the bulk metal, therefore assuming that the slab is in equilibrium with the bulk, which acts as the reservoir.

In taking the difference between the Gibbs free energy of the surface adsorbate system and the reference clean slab, there will be some cancelation of vibrational contributions (e.g. from the bulk and some surface contributions). However, the contribution due to atomic or molecular adsorbates, which are not present in the reference system, must be carefully checked. In some cases, e.g. involving adsorption of water, the contributions can be significant [22]. For a number of O/TM systems however (e.g. O/Ag(111) [21] and O/Cu(111) [23]), it has been found that these effects are sufficiently small as not to play an important role in the conclusions. If this is the case, the Gibbs free energy difference can be approximated by the difference of the total energy terms as obtained by first-principles calculations. The temperature (T) and pressure (p) dependence is mainly given by μ_{O}, i.e. by the O_2 gas phase atmosphere, where

$$\mu_{\mathrm{O}}(T, p) = 1/2\left[E_{\mathrm{O_2^{total}}} + \tilde{\mu}_{\mathrm{O_2}}(T, p^0) + k_{\mathrm{B}}T\ln\left(\frac{p_{\mathrm{O_2}}}{p^0}\right)\right]. \tag{2}$$

Here p^0 is atmospheric pressure and $\tilde{\mu}_{\mathrm{O_2}}(T, p^0)$ includes contributions from rotations and vibrations of the molecule, as well as the ideal gas entropy at 1 atm. It can be taken from experimental values listed in thermodynamic tables [24] (the choice made in the studies presented here) or directly calculated. For a given atomic configuration, $\Delta G(\mu_{\mathrm{O}})$ can then be plotted as a (linear) function of the oxygen chemical potential, where the greater the amount of oxygen that is accommodated in the surface structure, the steeper the slope of the line. In the limiting case of the bulk oxide, the line will become vertical at a value of the oxygen chemical potential that equals the bulk oxide heat of formation per O atom. From consideration of many conceivably relevant

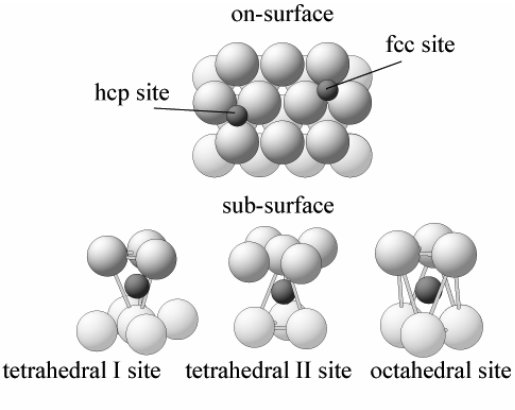

Figure 1. Highly coordinated adsorbate sites at an fcc(111) or hcp(0001) surface. Upper: top view of the surface where the two threefold coordinated hollow sites are indicated. Lower: local atomic geometries of three high-symmetry subsurface interstitial sites under the first substrate layer. Metal and oxygen atoms are shown as large and small spheres, respectively.

surface atomic configurations, those with the lowest surface free energy of adsorption, for a given value of the oxygen chemical potential, can be identified. The approach of *ab initio* atomistic thermodynamics is clearly applicable to all solid surfaces, and it has been used to study, e.g., hydrogen on gallium nitride surfaces [25], and numerous other systems as well. It should be mentioned that obviously this is an indirect approach, and a limitation is that its reliability is restricted to the structural configurations considered. If the really most stable phase is not included in the set of structures considered, the approach will not find it, although the obtained phase diagram may well give some guidance to what other structures one could and should test as well. Furthermore, the approach cannot describe disordered phases, which may become important e.g. at more elevated temperatures; if this is the case then an explicit calculation of the configurational entropy contribution will become necessary, which can be addressed by equilibrium Monte Carlo simulations.

In the present paper we will also discuss the average binding energy of oxygen on a surface, which is defined as

$$E_{\mathrm{b}} = -\frac{1}{N_{\mathrm{O}}}\left[E_{\mathrm{O/Surf}} - E_{\mathrm{Surf}} - N_{\mathrm{O}}E_{\mathrm{O}} - \Delta N_{\mathrm{M}}E_{\mathrm{M}}\right], \qquad (3)$$

where $E_{\mathrm{O/Surf}}$, E_{Surf}, E_{O} and E_{M} are the total energies of the adsorbate system, the corresponding clean surface, the free oxygen atom and a bulk metal atom, respectively. A positive adsorption energy reflects that the adsorption is exothermic. Plotting this quantity as a function of coverage affords the determination of the relative stability of various adsorption sites and structures for a specified coverage (e.g. on-surface versus subsurface adsorption), as well as such a comparison across the considered transition metal substrates. It also provides insight into which metastable structures may be observed should a system be kinetically hindered from reaching the ground state configuration.

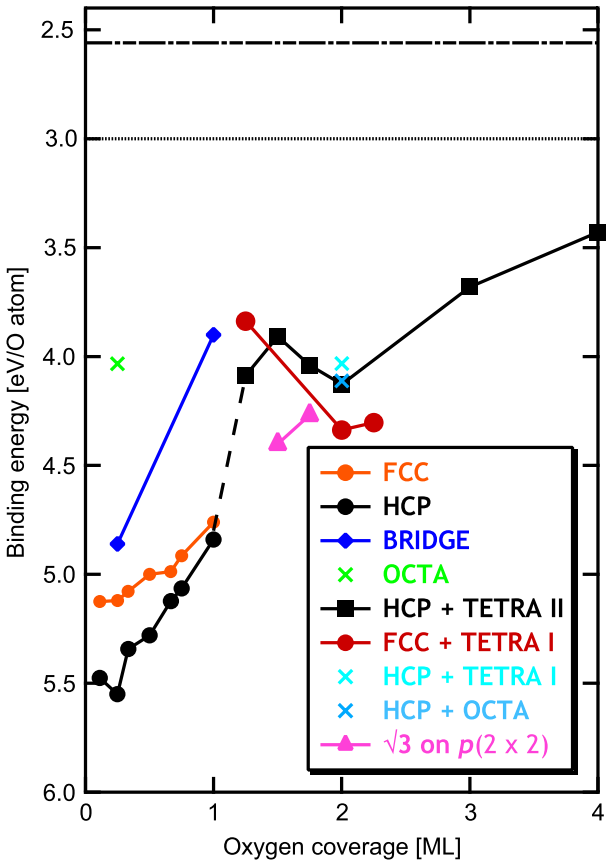

Figure 2. Average binding energies of oxygen on Ru(0001) for various on-surface and 'mixed' on-surface + subsurface geometries, and surface-oxide-like structures (e.g. '$\sqrt{3}$ on p(2 × 2)'). The horizontal upper and lower lines correspond to half the experimental and theoretical O_2 binding energies, respectively. (Adapted from [33, 35, 36].)

3. Transition metals, Ru, Rh, Ir, Pd

3.1. The oxygen–ruthenium (0001) system

The interaction of oxygen with Ru(0001) was one of the first O/TM systems to attract significant attention of theoretical and experimental studies. The motivation stems from the observation that supported Ru catalysts [26], as well as Ru(0001) single crystals [27], have a high reactivity for CO oxidation under high pressure and temperature conditions; however, under UHV conditions [28], the turnover frequency is extremely low. This system thus exhibits a clear 'pressure and temperature gap' and begs the question as to what the underlying reasons for this phenomenon are, on the microscopic level [29].

We first consider the average binding energy of oxygen on Ru(0001) as a function of coverage. Various on-surface adsorption sites have been considered, namely fcc- and hcp-hollow and bridge sites, as well as sites involving both on-surface and subsurface sites. In figure 1 these various sites are illustrated. In addition, a configuration that can be described as a $(\sqrt{3} \times \sqrt{3})$R30° O–Ru–O 'trilayer' on a (2 × 2) Ru(0001) surface unit cell (labeled '$\sqrt{3}$ on $p(2 \times 2)$') was considered. This structure was stimulated by a similar structure

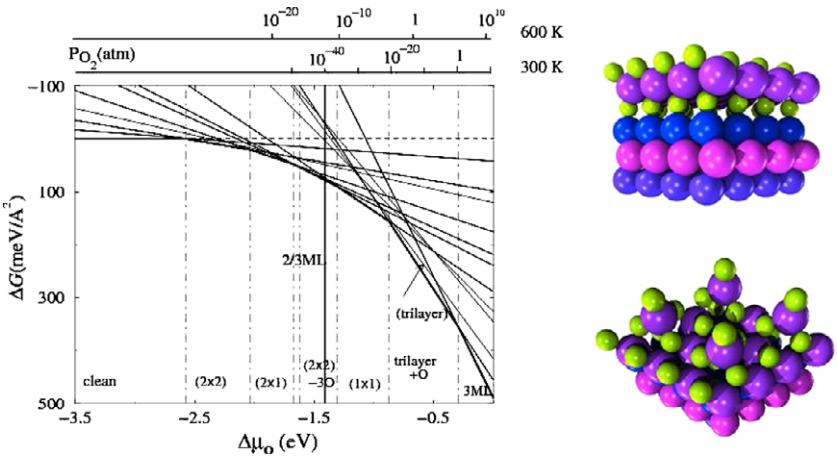

Figure 3. Calculated surface free energy of adsorption for low energy O/Ru(0001) structures. The oxygen chemical potential is given with respect to half the total energy of the free oxygen molecule. The various stable phases are listed along the bottom of the plot, where the label '2/3 ML' indicates the $(\sqrt{3} \times \sqrt{3})$R30°-2O structure, which is only stable for a very narrow region of the oxygen chemical potential. The favorable surface phases are (2×2)-O, (2×1)-O, $(\sqrt{3} \times \sqrt{3})$R30°-2O, (2×2)-3O, (1×1)-O, and the 'trilayer + O' configuration (see right, lower figure). The structure of the 'trilayer' configuration is shown to the right (upper figure). The three thin lines for the structures not labeled are less stable structures and correspond to chemisorbed O at 0.33 ML, and the trilayer-like $(\sqrt{3} \times \sqrt{3})$R30° configuration on a (2×2) surface unit cell configuration with and without an O atom adsorbed on top. The vertical continuous line marks the theoretical heat of formation of RuO_2 per O atom. Reproduced with permission from [35].

being observed for the O/Rh(111) system (described below). Figure 2 shows the results for the average binding energy, which were obtained using the pseudopotential [30] plane-wave method [31] and the generalized gradient approximation (GGA) of Perdew *et al* [32].

It can be seen from figure 2 that Ru binds O strongly to the surface. The binding energy is the greatest of the O/TM systems considered here. It can also be noticed that oxygen is stable on the surface with respect to free O_2 right up to a full monolayer coverage, and still exothermic up to 4 ML. For coverages in excess of 1 ML, DFT-GGA calculations have been carried out for many atomic configurations involving on-surface O in fcc and hcp sites, and the three subsurface sites [33, 34], i.e. for various 'mixed' on-surface + subsurface configurations in (2×2) surface unit cells. The most favorable of these are included in figure 2. Occupation of subsurface sites yields a rapid decrease in the energy, as can be seen from the structures with coverage > 1 ML. At a total coverage of 2 ML, the average binding energy of this structure, which corresponds to a monolayer of O in fcc sites and a monolayer in tetra I sites, is very similar to that corresponding to the same structure, but with the adsorption of an additional O atom on top of a surface Ru atom (yielding coverage 2.25 ML), as well as to the heat of formation of RuO_2 (per O atom). It is also very similar to the $(\sqrt{3} \times \sqrt{3})$R30° O–Ru–O 'trilayer' structure on a (2×2) Ru(0001) (labeled '$\sqrt{3}$ on p(2×2)') in figure 2, with and without an additional O adsorbed on the surface Ru atoms. These latter two structures have coverages corresponding to 1.5 and 1.75 ML.

In figure 3 the surface free energy of adsorption is shown as a function of the oxygen atom chemical potential for the low energy structures contained in figure 2. It can be seen that a sequence of chemisorbed phases is predicted to be stable before bulk RuO_2 becomes energetically preferred (at $\mu_O = -1.4$ eV). Specifically, for $\mu_O < -2.7$ eV the clean surface is most stable, while five different O adsorbate phases (with oxygen occupying the hcp site) with increasing coverage become progressively stable for more O-rich environments, namely (2×2), (2×1), $(\sqrt{3} \times \sqrt{3})$R30°-2O (for a very small range of μ_O), (2×2)-3O, and (1×1). All of these structures have been experimentally verified, with the exception of the $(\sqrt{3} \times \sqrt{3})$R30°-2O configuration. For $\mu_O > -1.4$ eV, bulk RuO_2 represents the most stable phase. The stability range of the bulk oxide is large, and it encompasses all realistically attainable pressures for temperatures below about 600 K, pointing to oxidized Ru metal being the active phase under typical (oxidizing) catalytic conditions, consistent with experiment [37]. Figure 4 shows STM images of the Ru(0001) surface resulting from being held in an oxidizing environment. The coexistence of patches on the surface of the 1 ML (1×1)-O phase with patches of bulk oxide can be clearly seen. If full thermodynamic equilibrium is not reached, i.e. if the system is kinetically hindered, surface-oxide-like structures could possibly be stabilized at the surface, such as the 'trilayer + O' configuration depicted to the right of figure 3. To date however, to our knowledge, no thin surface-oxide-like structures have been reported to form on Ru(0001).

3.2. The oxygen–rhodium (111) system

For oxygen adsorption on Rh(111), a number of ordered phases have been experimentally identified, including (2×2) and (2×1) structures for coverages 0.25 and 0.50 ML, respectively [38], as well as $(2\sqrt{3} \times 2\sqrt{3})$R30° and (2×2)-3O phases [39], and the (1×1)-O structure [40]. In these configurations, the oxygen atoms occupy the on-surface hollow sites. For higher oxygen exposures, a structure with a periodicity close to (9×9) is observed [41]. This phase

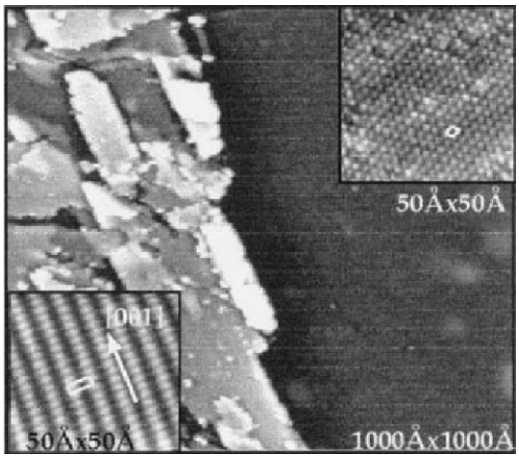

Figure 4. STM images of oxygen on Ru(0001). On the right is the (1 × 1)-O/Ru(0001) phase, where, in the magnified inset, the hexagonal Ru(0001) lattice can be seen. The dark spots mark the locations of the chemisorbed O atoms. On the left side $RuO_2(110)$ domains are visible. The magnified inset shows the structure of this phase and its rectangular unit cell. Reprinted with permission from [37].

gives rise to a moiré pattern, which may be understood as corresponding to a hexagonal overlayer on the (111) substrate, which has a larger in-plane distance. Studies employing scanning-tunneling microscopy (STM) and high resolution core-level spectroscopy, together with DFT calculations (using the VASP code [43]), have characterized the O/Rh(111) system. In particular, the '(9 × 9)' phase, which can be described as an (8 × 8) hexagonal surface oxide on a (9 × 9) Rh(111) surface unit cell, is proposed to correspond to a trilayer type of surface oxide [41] (see figure 6(b)).

Figure 5 shows the average binding energy as a function of coverage. At 0.25 ML, the value of ∼5.25 eV is somewhat lower than for O on Ru(0001) at the same coverage. Similarly to O/Ru(0001) (and all other O/TM systems presented here), the average binding energy decreases with increasing coverage, reflecting an effective repulsive adsorbate–adsorbate interaction. Structures involving pure subsurface oxygen are notably less stable than on-surface configurations. The average binding energies of the surface-oxide-like structures '($\sqrt{3}$ on $p(2\times2)$)' used to simulate the incommensurate '(9×9)' phase are notably more favorable than those considered involving on-surface + subsurface configurations (e.g. fcc + octa).

The phase diagram is shown in figure 6(a). It is quite striking that the calculations show that the surface oxide is only *metastable* with respect to bulk oxide formation. Thus, this phase is 'kinetically stabilized'; that is, notable energy activation barriers prevent the system from reaching thermal equilibrium under the experimental conditions. This was actually also the case for the $(2\sqrt{3}\times2\sqrt{3})$R30° and (2 × 2)-3O structures [39], as well as the (1 × 1)-O phase, which are metastable. DFT calculations reveal that the stability of the (8 × 8) oxide-like structure, calculated in a (9 × 9) surface unit cell, is actually very similar to that obtained for the structure calculated using a smaller (2 × 2) surface unit cell, where the configuration could then be described as having a $(\sqrt{3}\times\sqrt{3})$R30° periodicity on a (2 × 2) surface unit cell.

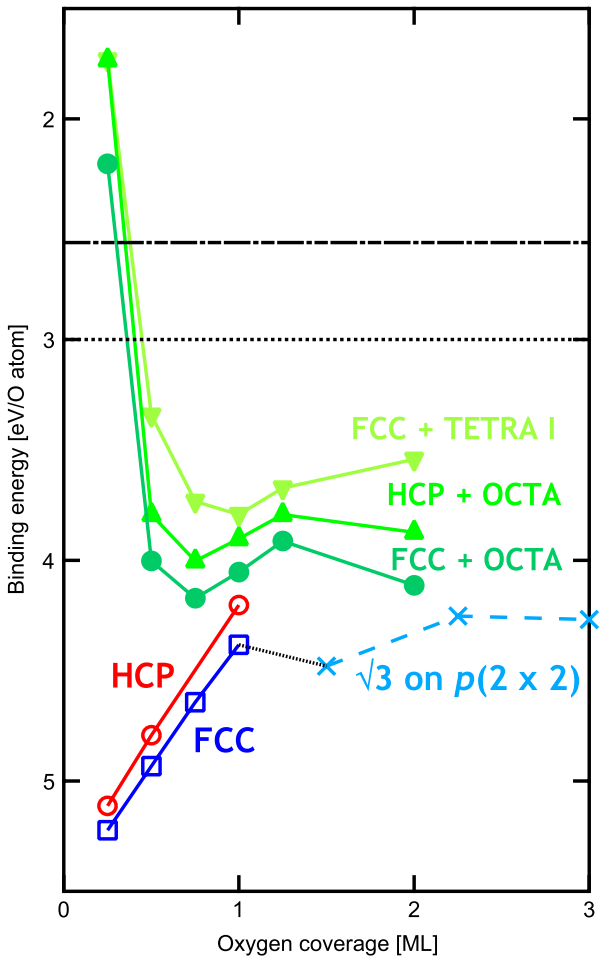

Figure 5. Average binding energies of oxygen on Rh(111), for on-surface, subsurface, and 'mixed' on-surface + subsurface structures, as well as surface-oxide-like configurations ('$\sqrt{3}$ on p(2× 2)'). The horizontal upper and lower lines correspond to half the experimental and theoretical binding energies of O_2, respectively. (Adapted from [41, 42].)

3.3. The oxygen–iridium (111) system

As a late 5d transition metal, iridium shows potential for a variety of applications, particularly as a heterogeneous catalyst in the chemical industry [44]. For example, Ir and Ir-alloy catalysts are widely used in reactions that require the activation of strong C–H bonds. Iridium has also been considered to improve the automobile catalytic converter because of its ability to decompose NO and to reduce NO_x with hydrocarbons [45]. Clearly, as for the other TMs it would be valuable to have a detailed atomic level understanding of the interaction of Ir with reactant gas environments, for example oxygen. In the present subsection we discuss our recent theoretical results for the O/Ir(111) system.

From the experimental side, the interaction of atomic oxygen with single-crystal Ir(111) surfaces has been the subject of several studies: low energy electron diffraction (LEED) [46] and ultraviolet photoelectron spectroscopy (UPS) studies showed that exposure of a clean Ir(111) surface to oxygen produces a (2 × 2) LEED pattern [47]. Such a pattern could either be caused by a $p(2\times2)$ surface structure or by

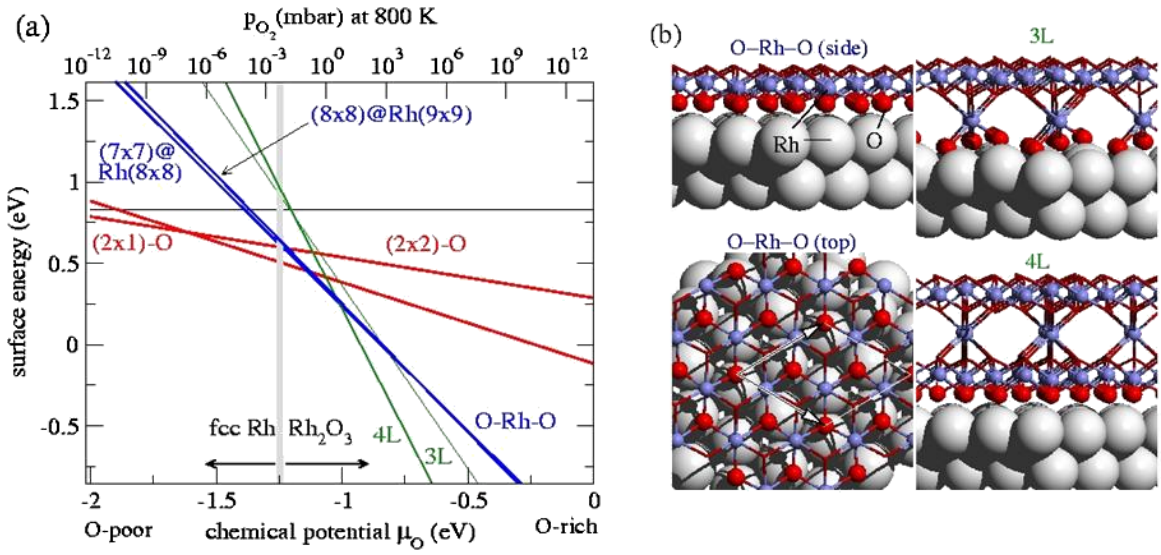

Figure 6. (a) Calculated surface free energy for various low energy structures of O on Rh(111) and (b) lowest energy structures for surface oxides with two (O–Rh–O), three, and four layers (L) of oxygen on a Rh(111) (2 × 2) surface unit cell. Oxygen atoms are shown as bonds only, except for the bottom oxygen layer. Reprinted figure with permission from [41]. Copyright 2000 by the American Physical Society.

three domains of a (1 × 2) surface structure rotated by 120° with respect to one another. The $p(2 \times 2)$ surface structure corresponds to a coverage of 0.25 ML, and the (1×2) structure to a coverage of 0.5 ML. X-ray photoelectron spectroscopy (XPS) and high resolution electron energy loss spectroscopy (HREELS) [48, 49] studies reported that 0.5 ML was the maximum coverage for atomic oxygen. A single chemisorbed state for atomic oxygen on Ir(111) was indicated from the observation of a single loss peak in EELS of 550 cm^{-1} at the saturation coverage [50].

Regarding first-principles investigations, the adsorption and dissociation of O_2 on Ir(111) has been studied, where it was found that the dissociation is nearly spontaneous, with a very small activation energy of 0.06 eV/O_2, consistent with experimental adsorption data [51]. Chemisorption of atomic O on Ir(111) was also considered in this theoretical study, where the preferred binding site, atomic structure and vibrational frequencies at 0.25 ML coverage were reported. This study found that atomic oxygen adsorbs preferentially in the threefold fcc-hollow site. *Ab initio* investigations of oxygen adsorption on Ir(111) have therefore hitherto been limited to a very narrow range of oxygen coverage, and to zero pressure and zero temperature.

Recently, we have performed first-principles investigations for atomic oxygen adsorption on Ir(111) for a wide range of oxygen coverages, θ, namely from 0.11 to 2.0 monolayers (ML), including subsurface adsorption and thin surface-oxide-like structures [52]. For these calculations we used the DMol^3 code and the GGA for the exchange–correlation functional. For on-surface adsorption, we considered hcp-and fcc-hollow sites, and bridge and on-top sites. We found that oxygen prefers the fcc-hollow site for all coverages considered, as can be seen from figure 7(A). Similarly to oxygen adsorption on other transition metal surfaces, as θ increases from 0.25 to 1.0 ML, the binding energy decreases substantially, indicating a repulsive interaction between the adsorbates. For the coverage range of 0.11–0.25 ML, there is an attractive interaction, indicating island formation with a (2 × 2) periodicity and a local coverage of 0.25 ML. The binding energy for $\theta = 0.25$ ML is ∼4.7 eV, which is weaker than for O/Rh(111) (∼5.25 eV) and for O/Ru(0001) (∼5.5 eV). Pure subsurface oxygen adsorption is found to be only metastable and endothermic with respect to the free O_2 molecule. For structures involving on-surface+subsurface sites (i.e. fcc + tetra I and hcp + octa) it can be seen that for coverage beyond 1 ML the incorporation of oxygen under the first Ir layer initially exhibits a decrease in the average binding energy due to the energy cost of distorting the substrate layers. For coverages from 1.5 to 2.0 ML, the energy becomes more favorable, indicating an attractive interaction between the O atoms, as found also for O/Ru(0001) and O/Rh(111). We also considered a surface-oxide-like structure as for the O/Ru(0001) and O/Rh(111) systems (i.e. a so-called '$\sqrt{3}$ on $p(2 \times 2)$' structure for $\theta = 1.5$ ML, see figure 6(b), labeled O–Rh–O) and find that it has the most favorable average binding energy at this coverage, as seen from figure 7(A) (here labeled '$p2$:IrO_2'). We also consider a similar structure, which is found to be less stable, where the O–Ir–O trilayer is laterally shifted such that the lower lying oxygen atoms occupy the high symmetry sites of the underlying (111) substrate (instead of the Ir atoms). It is labeled as '$p2$:IrO_2-SR'.

Through calculation of the surface Gibbs free energy of adsorption (figure 7(B)), and taking into account the temperature and pressure via the oxygen chemical potential, we obtain the (p, T) phase diagram of O/Ir(111) as shown in figure 7(C). These results show that for practically all conditions, except for UHV and high temperatures, the bulk oxide is thermodynamically the most stable phase. The (2×2)-O structure with $\theta = 0.25$ ML is the only chemisorbed phase that is predicted to be stable on the surface, and only for a very narrow range of the oxygen chemical potential, which may be achievable under UHV conditions. These results suggest that

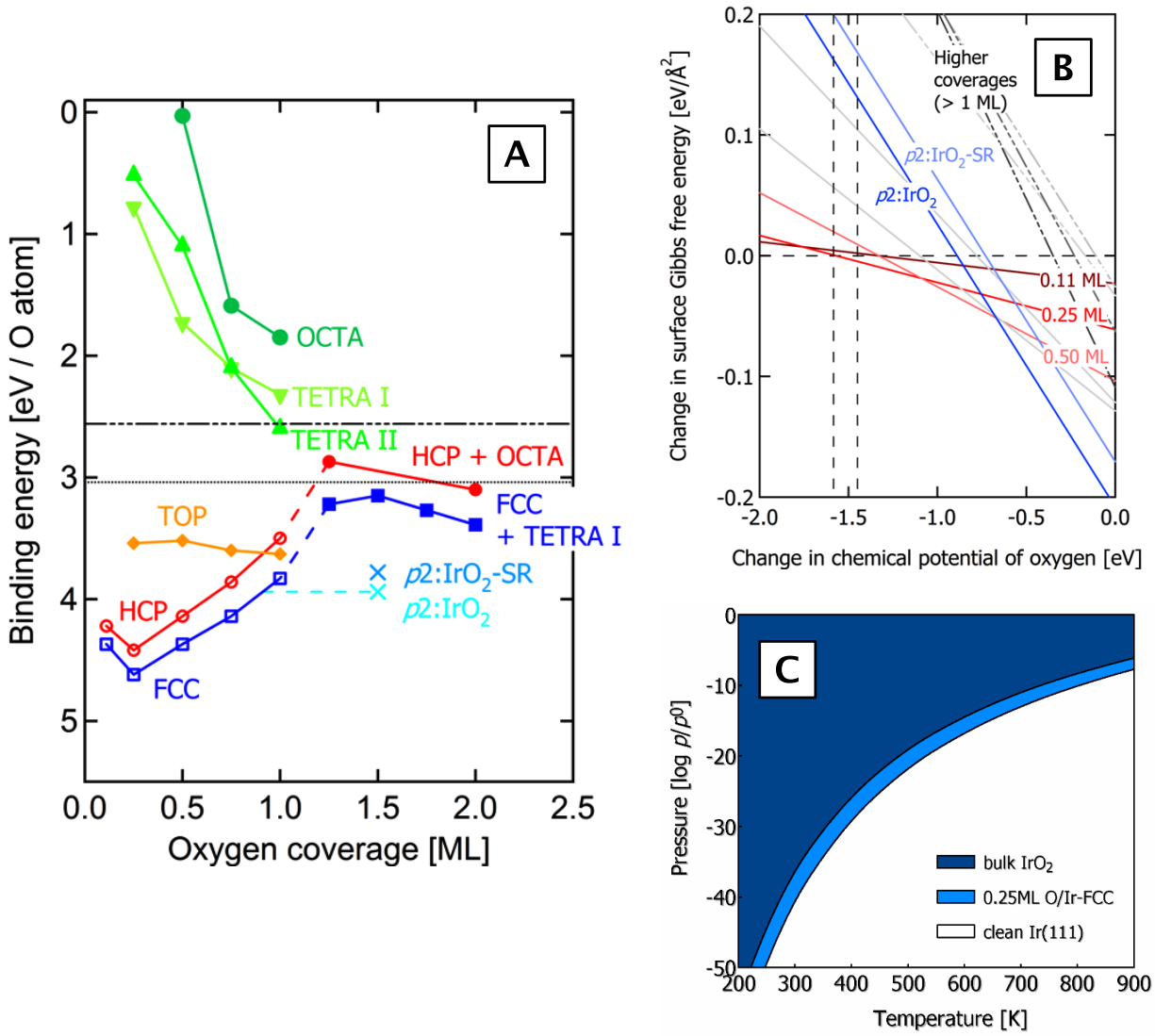

Figure 7. (A) Average binding energies of oxygen on Ir(111) for the fcc- and hcp-hollow sites, as well as on-top sites, and the three subsurface sites. Also shown are results for on-surface + subsurface sites (i.e. hcp + octa and fcc + tetra I) and a surface-oxide-like structure (labeled e.g. '$p2$:IrO_2') that can be described as a $(\sqrt{3} \times \sqrt{3})$R30° trilayer O–Ir–O structure on a (2 × 2) surface unit cell. The upper and lower horizontal lines indicate half the experimental and theoretical binding energies of O_2, respectively. (B) Gibbs free energy of adsorption for the various low energy structures; (C) the stability range of the lowest energy structures considered in B, shown in (p, T)-space. (Adapted from [52].)

the experimentally reported (2 × 2) phase for coverage 0.5 ML could actually have coverage 0.25 ML, or that the phase (if the coverage is actually 0.5 ML) is only metastable with respect to bulk oxide formation. We note that in an atmosphere which contains reducing species as well as oxidizing the predicted stability region of bulk oxide formation is expected to be reduced.

3.4. The oxygen–palladium (111) system

Recently the formation of one-layer surface oxides has been reported on Pd(111) through a combination of STM and DFT studies [53]. Interestingly, in addition to the 'Pd_5O_4' structure determined previously [54], six different structures have been observed and characterized [53], thus underlining the complex nature of surface oxides at certain TMs. These oxides form under oxygen-rich conditions, near the thermodynamic stability limit of PdO bulk. The structures are denoted as 'Pd_9O_8', '$Pd_{20}O_{18}$', '$Pd_{23}O_{21}$', '$Pd_{19}O_{18}$', 'Pd_8O_8', and '$Pd_{32}O_{32}$'. All contain oxygen atoms that form a rectangular lattice and a favorable alignment to the Pd(111) substrate.

To compare the behavior of this system with the other O/TM systems, we first consider the average binding energy as a function of coverage, which is shown in figure 8. At $\theta = 0.25$ ML, the value is ∼4.5 eV, which is less than that on Rh(111) (∼5.25 eV), Ir(111) (∼4.7 eV), and Ru(0001) (∼5.5 eV). As for the other fcc metal systems, O/Rh(111) and O/Ir(111), adsorption in the hcp site is less favorable than the fcc site for the range of coverages up to full ML. Similarly, the pure subsurface sites are significantly less stable. As for

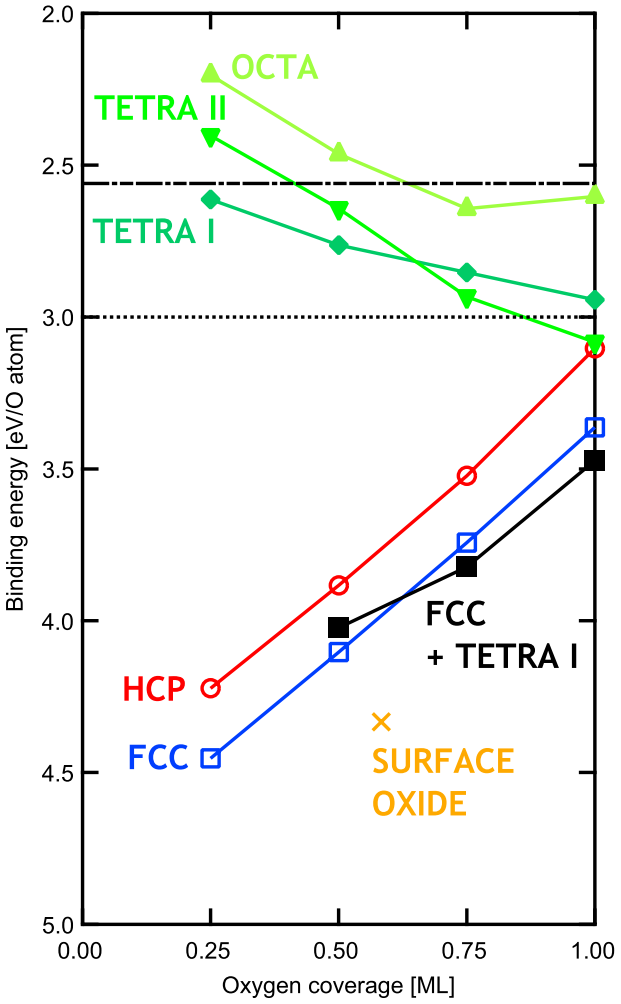

Figure 8. Average binding energy of oxygen on Pd(111) with respect to the free O atom, as a function of coverage. On-surface hcp- and fcc-hollow sites, as well as pure subsurface sites, are considered. Also results for structures involving on-surface+subsurface, as well as that for the so-called '$(\sqrt{6} \times \sqrt{6})$' structure, used to simulate the incommensurate surface oxide, are included. The upper and lower horizontal lines indicate half the experimental and theoretical binding energies of O_2, respectively. (Adapted from [54–56].)

the previous O/TM systems, 'mixed' on-surface+subsurface geometries have been considered, consisting of on-surface O in fcc sites and subsurface O in the tetra I sites (labeled 'fcc + tetra I' in figure 8). The average binding energies of these structures are slightly more favorable than for the on-surface chemisorbed structures at the same coverage. However, it can be seen that the average binding energy of the so-called '$(\sqrt{6} \times \sqrt{6})$' pseudo-commensurate surface oxide structure, which has been identified [54] on the basis of experimental and theoretical studies, has a significantly lower energy than any of the mixed structures. On considering the surface free energy, as shown in figure 9 (left), it can be seen that this configuration is a *thermodynamically stable* phase for a small range of the oxygen chemical potential. From figure 9, as a function of increasing oxygen chemical potential, it can be observed that firstly, after the clean Pd(111) surface, on-surface, chemisorbed oxygen is predicted to be stable with a p(2 × 2) periodicity, followed by formation of the '$\sqrt{6}$' thin surface-oxide-like structure, and then bulk palladium oxide. Interestingly, as noted above, many other surface-oxide-like configurations have been identified [53], which all have rather similar energies (as shown in figure 9, left), but which are less stable than the '$\sqrt{6}$' structure. Despite their higher energies, the STM experiments show that these phases form, and can coexist at the surface (see figure 9, right), highlighting the very complex nature and behavior of the O/Pd(111) system.

For the O/Pt(111) system, experiments have reported that the thermal stability of a surface Pt oxide on Pt single crystal surfaces significantly exceeds that of bulk PtO_2 [57], and furthermore that structurally similar oxides develop on both Pt(111) and Pt(100). While there have been a number of recent first-principles investigations into the stability of surface oxides at Pt(110) and Pt(100), much fewer have been reported on Pt(111). One *ab initio* study that has been performed reported that the most stable superficial oxide phase is a thin layer of α-PtO_2 on the surface [58].

4. Oxidation of coinage metal surfaces, Cu, Ag, Au

The coinage metals—copper, silver and gold—are well known for their intrinsic catalytic properties, especially in (partial) oxidation reactions. Although traditionally mistaken for their 'nobility' and 'chemical inertness', these metals are now validated as excellent catalysts for industrially important chemical reactions such as the partial oxidation of methanol, the low temperature water–gas shift (WGS) reaction [85] and the low temperature preferential oxidation (PrOx) of carbon monoxide [12, 59–68]. In recent years, there has been a great focus on clean renewable energy technology, bringing about a renewed interest in the above-mentioned chemical reactions, in relation to fuel-cell powered vehicles, where hydrogen is obtained via partial oxidation and steam reforming of hydrocarbons and methanol [61]. The hydrogen fuel is also further purified via the WGS and PrOx reaction to prevent the poisoning of the platinum electrodes found in fuel cells. To date, extensive results from classical surface science experiments have taught us a great deal about these systems under UHV conditions. However, to gain insight into the function of these metals as oxidation catalysts, it is necessary to extend our understanding to elevated temperatures and pressures, similar to those of real catalysis. In the present section we focus on the fundamental study of the oxygen–metal interaction at the interface of an oxygen atmosphere and the thermodynamically most stable metal surface, i.e. O/M(111) systems, where M is Cu, Ag and Au.

We will first briefly survey the homogeneous chemisorbed phases and then concentrate on the formation of so-called surface oxide structures on these coinage metal surfaces. Employing the concept of *ab initio* atomistic thermodynamics [35] as before, we will also discuss the relative stability of different surface phases under both ultra-high vacuum (UHV) and for more realistic technical catalysis conditions.

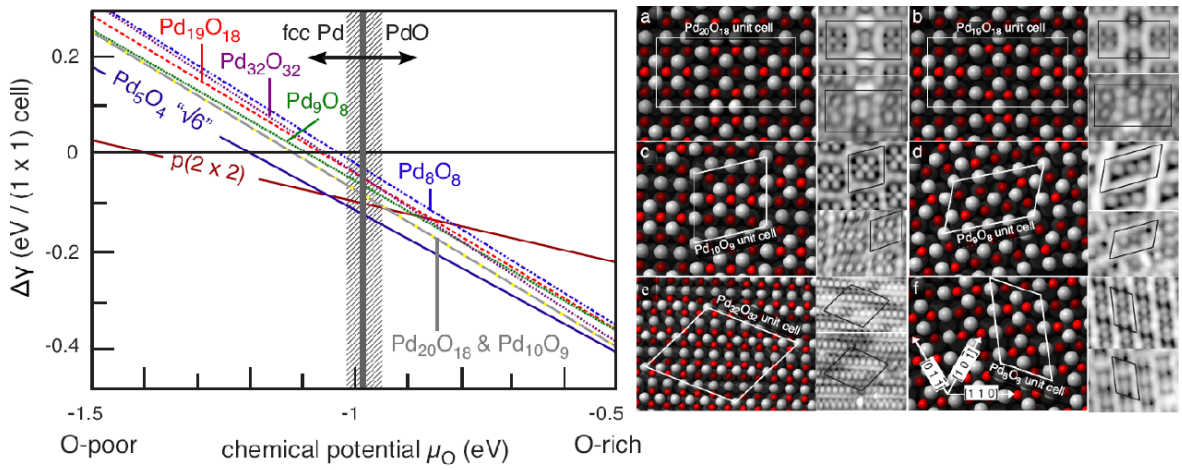

Figure 9. Left: surface free energy for various low energy structures of oxygen on Pd(111). The vertical black line indicates the border of the PdO stability regime above ∼−1 eV. The dashed area indicates the experimental preparation conditions. Right: atomic geometry and STM images of the many surface-oxide-like phases identified. Reprinted figure with permission from [53]. Copyright 2007 by the American Physical Society.

4.1. The oxygen–copper (111) system

The O/Cu(111) system is often used as a model to study copper-based catalysts and has been investigated both theoretically [23, 69, 70] and experimentally [71–82]. Although all these studies agree that a disordered chemisorbed phase forms on Cu(111), the exact microscopic structure is still not known. The earliest structural study was conducted by Niehus using low energy ion scattering (LEIS) [75]. A lateral displacement of surface copper atoms was reported, accompanied by the formation of a 'rough' oxygen overlayer with a corrugation of ∼0.3 Å. Two later studies, using surface-extended x-ray absorption fine structure (SEXAFS) spectroscopy [76] and surface extended-energy-loss fine structure (SEELFS) spectroscopy [77], attempted to determine the local environment of the chemisorbed oxygen species and found it occupies a threefold hollow site. It was considered that this oxygen species could have partially penetrated the surface layer, causing a lateral displacement of the copper atoms near the hollow sites and thus explaining the roughened surface structure seen. Subsequently, Jensen *et al* [79] proposed an improved model, which suggested that the former chemisorbed phase mentioned above was inadequate. This proposed, rather complex, model was based on the mismatch-overlayer structure of the (111) face of Cu_2O and the metal surface. More recent scanning-tunneling microscopy (STM) [71] and normal incidence x-ray standing wavefield absorption (NIXSW) [80] studies confirmed a similar pseudo-Cu_2O overlayer structure to that proposed in [79] (see figures 11(C) and (D)).

To date, classical surface science experiments have shed much light on the fundamental physics and chemistry of O/Cu(111). However, to bridge our understanding of the behavior of the O/Cu(111) system to the conditions of elevated temperature and high pressure it is crucial to consider the surface structure in an oxygen atmosphere.

We have recently studied the O/Cu(111) system using DFT calculations, with the DMol^3 code [83], employing the GGA [84], where we initially surveyed different homogeneous chemisorbed oxygen overlayers on Cu(111) (see figure 10). Similar to the other O/TM systems discussed so far, we found the threefold hollow fcc site to be energetically most favorable, with a binding energy of ∼4.65 eV, at an oxygen coverage of 0.25 ML, thus rather similar to O/Pd(111) (∼4.5 eV) and O/Ir(111) (∼4.7 eV). We also find that pure subsurface oxygen adsorption is notably less stable than on-surface adsorption, but for coverage ∼0.8–0.9 ML the octa site becomes more stable [23]. Guided by experimental observations [71, 79], we investigated various oxidic structures on Cu(111). Specifically, these structures contain a trilayer (i.e. a layer of oxygen atoms, followed by a layer of copper atoms, and another layer of oxygen atoms) with a similar geometry to the hexagonal (111) surface of bulk Cu_2O. The atomic structure of selected low energy oxidic surfaces are shown in figure 11(E), and their average binding energies in figure 10. It is interesting to note from figure 10 that these oxidic structures or 'surface oxides' are energetically very similar to the most stable energy simple chemisorbed phases at very low coverages, even though their atomic structures are vastly different. This indicates that the energy gained by forming these surface oxide structures outweighs the energy cost to reconstruct the (111) surface.

Using the calculated binding energies, we determine the surface free energy of adsorption as shown in figure 11(A) and the (p, T) phase diagram in 11(B). It can be seen that the calculations predict that the bulk oxide phase is the most stable for a wide range of oxygen pressures, from 10^{-10} and higher, and for all temperatures up to 700 K [23]. They also show that the thin surface-oxide-like structures are predicted to be stable in a region corresponding to UHV conditions, and chemisorption on the surface, at any coverage, is only metastable.

4.2. The oxygen–silver (111) system

A number of theoretical studies aimed at identifying the active oxygen species on Ag(111) involved in important chemical reactions such as ethylene epoxidation have been conducted in recent years (see e.g. [65, 66, 86] and references therein).

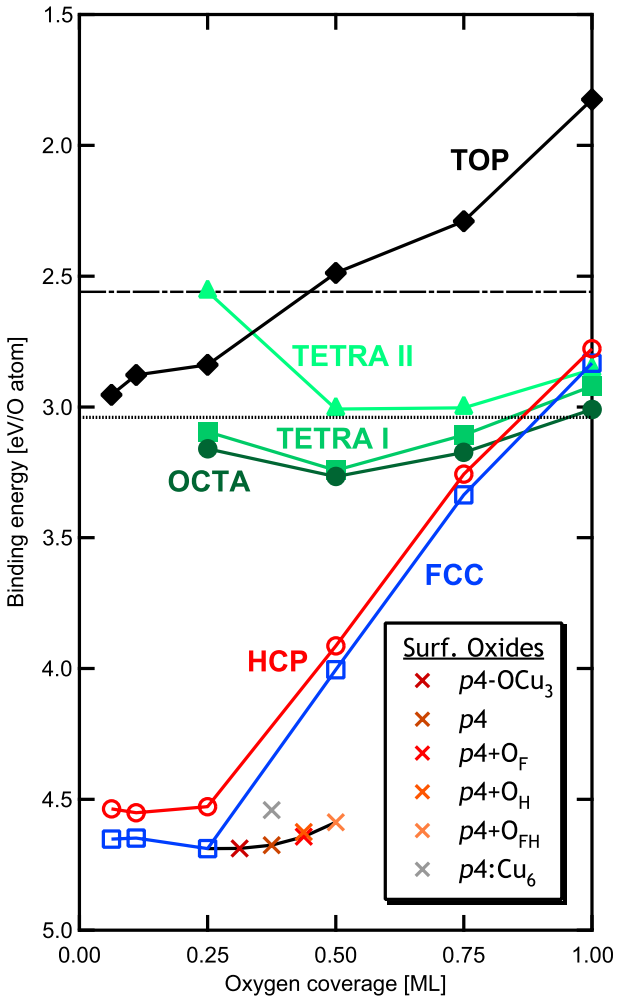

Figure 10. Average binding energies of oxygen on Cu(111) for homogeneous chemisorption phases, the three subsurface sites, and the energetically most favorable surface oxides as a function of oxygen coverage, with respect to the energy of a free oxygen atom. The solid lines connecting the calculated binding energies are used to guide the eye. Half the binding energy of O_2, theory and experiment, is indicated by the dotted and dot–dashed horizontal lines, respectively. (Adapted from [23].)

In particular, attempts to better understand this system were undertaken by both Michaelides *et al* [87–89] and Li *et al* [66, 90–92]. Both independent studies investigating various oxidic structures came to the same conclusion, that thin Ag_2O (111)-like surface oxides with a $p(4 \times 4)$ surface periodicity were more stable than either the bulk oxide or adsorbed oxygen, and could play a role in the catalytic reactions. A good overview of the past and present work on this O/Ag system is provided by Michaelides *et al* [65], in which the authors also extend their previous works, and identify a host of other related low energy surface oxide-like structures.

More recently, two independent, combined experimental and theoretical studies reported a new structural model for the oxygen-induced $p(4 \times 4)$ reconstruction, which shows considerably better agreement with experimental results than all previously proposed models [93, 94]. The energetic stability of this new structure was found to be similar to [94] and actually less favorable than [93], the most stable earlier model, leading the latter authors to suggest that this may be due to the neglect of van der Waals interactions in the stabilization of oxygen-induced surface reconstructions of noble metals. Taking this 'simple' model system as an example, it only goes to show that the characterization of surface structures under elevated pressure and temperature conditions can be much more complicated than anticipated. This is also reflected in the many structures identified recently for the O/Pd(111) system [53].

For comparison with the other O/TM systems, we show in figure 12(A) the average binding energy of atomic oxygen for various structures, including on-surface and subsurface as well as 'mixed' structures involving both on-surface and subsurface O. In addition, the energetics for various (4×4) surface-oxide-like configurations are also shown. It can be seen that at low oxygen coverage ($\leqslant$0.06 ML) O prefers to adsorb on the surface in the fcc site. For coverage of 0.25 ML, the binding energy is only ~3.6 eV, notably weaker than for the O/Pd(111) (~4.7 eV) and O/Cu(111) (~4.65 eV) systems. With increasing oxygen coverage, the thin $p(4 \times 4)$ 'Ag_2O-asym' surface oxide is favored. For slightly higher coverage, the '$Ag_{1.5}O$' structure is favored (the same as that labeled '$Ag_{1.33}O$' in [65]), followed by the same structure, but with two additional O atoms adsorbed in the hollow sites of the (4×4) cell (labeled '$Ag_{1.5}O + 2O$'). For higher O concentrations, thicker oxide-like structures with coverage 0.25 ML on the surface and 0.50 ML between each Ag layer are most favorable of those considered. These results correlate well to the general behavior found experimentally in the early work of Czanderna [95], which shows that the average heat of adsorption of oxygen on silver powder decreases from 0.91 to 0.37 eV per oxygen atom (with respect to half the binding energy of O_2), and then remains constant at ~0.40 eV per oxygen atom for coverages $\Theta = 0.33$ to about 0.90 ML. This observation was attributed to the growth of an oxide layer.

To incorporate the effects of temperature and pressure, the change in the Gibbs free surface energy as a function of the change in the oxygen chemical potential is calculated and shown in figure 12(B). The results predict that for low values of the O chemical potential the clean Ag(111) surface is thermodynamically stable, while for increasing values there is a narrow region when on-surface O is most stable. For higher values of the chemical potential, thin surface-oxide-like structures are predicted to form over a relatively wide range, followed by onset of bulk oxide formation at a value of ~0.32 eV. Using the correlation of the oxygen chemical potential to p–T scales, the results in figure 12(B) are translated into a (p, T) phase diagram shown in figure 12(D), which describes the stable surface phases from UHV to high pressure conditions.

From the phase diagram [66] (figure 12(D)), it can be seen that at $p_{O_2} = 1$ atm and $T = 530$ K (i.e. around the catalytic conditions for ethylene epoxidation), and even down to 10^{-3} atm, surface oxides predominate in the O–Ag(111) system and are thermodynamically favored over homogeneous chemisorbed phases. In particular, under UHV conditions, chemisorption of oxygen on Ag(111) with low coverage (less

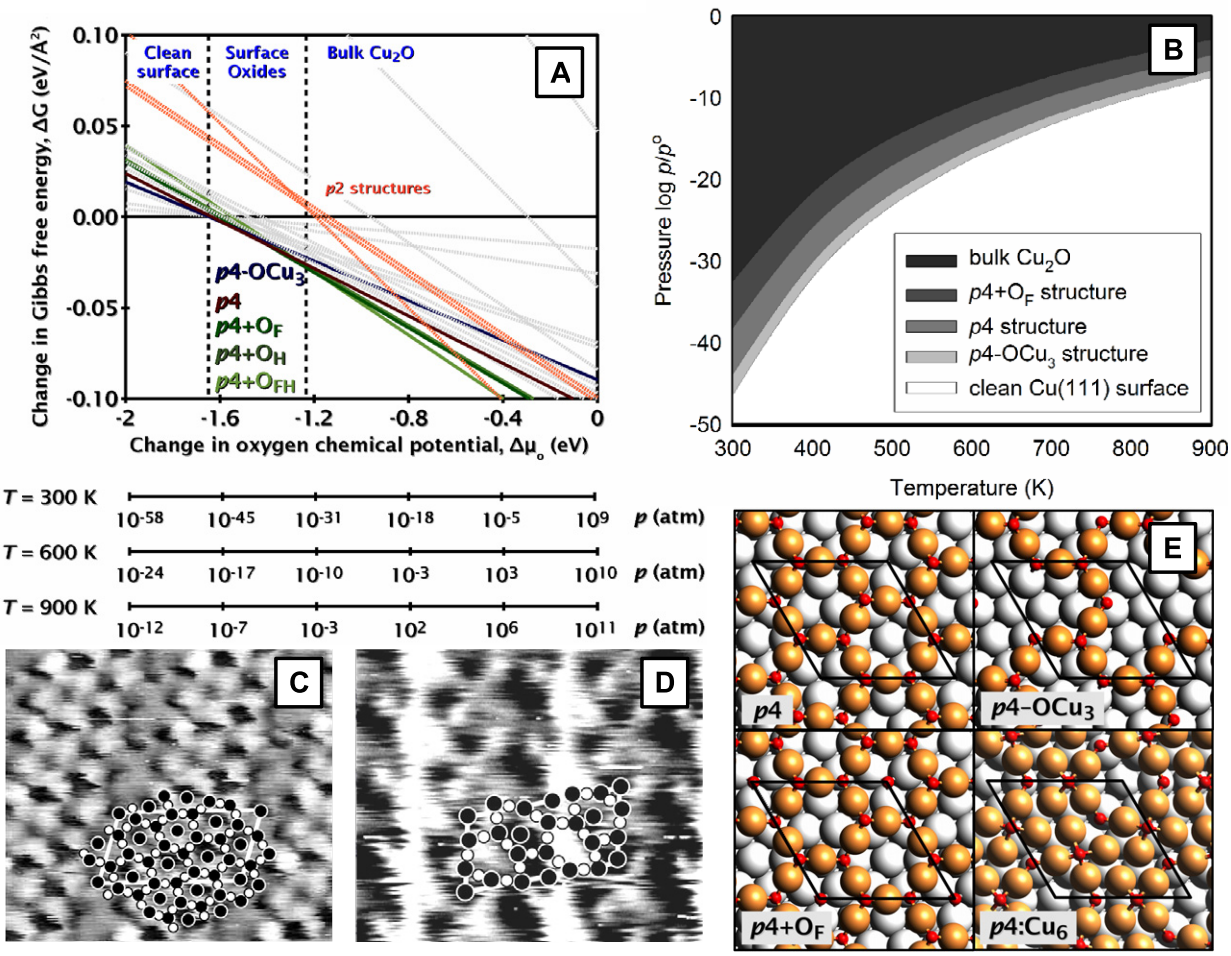

Figure 11. (A) Calculated Gibbs free energy of adsorption (relative to clean Cu(111) surface) of low energy oxidic structures as a function of the oxygen chemical potential (given with respect to half the total energy of the O_2 molecule) [23]. (B) The stability range of the most favorable structures evaluated in (A), plotted in (p, T)-space. (C), (D) The experimental STM images of proposed oxidic structures on Cu(111), namely the ($\sqrt{73}$R5.8° × $\sqrt{21}$R10.9°) structure (also known as the '44'-structure) and the ($\sqrt{13}$R46.1° × 7R21.8°) structure (also known as the '29'-structure), respectively. Reprinted from [71] with permission. Copyright 2001 from Elsevier. (E) Low energy surface oxidic structures considered for O/Cu(111), where the (4 × 4) surface unit cell is indicated. The underlying Cu substrate layer is shown as large pale gray spheres, with the Cu atoms in the oxide layer shown as large darker (orange) spheres. Oxygen atoms are represented by small dark (red) circles.

than 0.0625 ML) is stable up to about 360 K. This agrees well with experimental results, where it has been found that, for temperatures less than 490 K, 0.03 ML of oxygen can be adsorbed on the Ag(111) surface [96]. Under UHV conditions, the calculations also predict the stability of the $p(4 \times 4)$ phase at the lower temperatures of 160 to 260 K. This is also in line with STM results obtained under UHV conditions at low temperatures, where atomic resolution images of the $p(4 \times 4)$ phase have been achieved [86] (e.g. see figure 12(C)). The $p(4 \times 4)$ phase, however, cannot be directly prepared under these conditions, as it is known from experiment that temperatures greater than 400 K are required in order for the necessary atomic rearrangement to take place. It is therefore clear that it is the kinetics that prevent the reconstruction and formation of this phase at low pressures and temperatures.

4.3. The oxygen–gold (111) system

In recent years, nanoparticles of gold on (reducible) metal oxides (e.g. see figure 14(d)) have been found to be very active for a number of important chemical reactions (see e.g. [12, 67, 68] and references therein). These findings have stimulated huge efforts to probe into the possible mechanisms responsible for the high catalytic activity, including studies of the nature of oxygen adsorption on gold surfaces [97]. Despite the huge effort, there are still many fundamental aspects that are unclear. For instance, some studies of CO oxidation on TiO_2-supported gold catalysts at very low temperatures (90 K) report that the active species is the oxygen molecule [98, 99], while recent experiments find it is atomic oxygen which reacts with CO in the temperature range of 65–50 K [100, 101]. Small Au nanoparticles containing low-coordinated surface Au atoms are postulated to play a pivotal role in enhancing the dissociation of O_2 as well as increasing the binding strength of some of the reactants [102–105]. In spite of all these findings, the mechanisms responsible for the enhanced reactivity of the gold nanoparticles are still under debate.

To add more insight into the interaction of oxygen with gold, we examined in particular the stability of thin

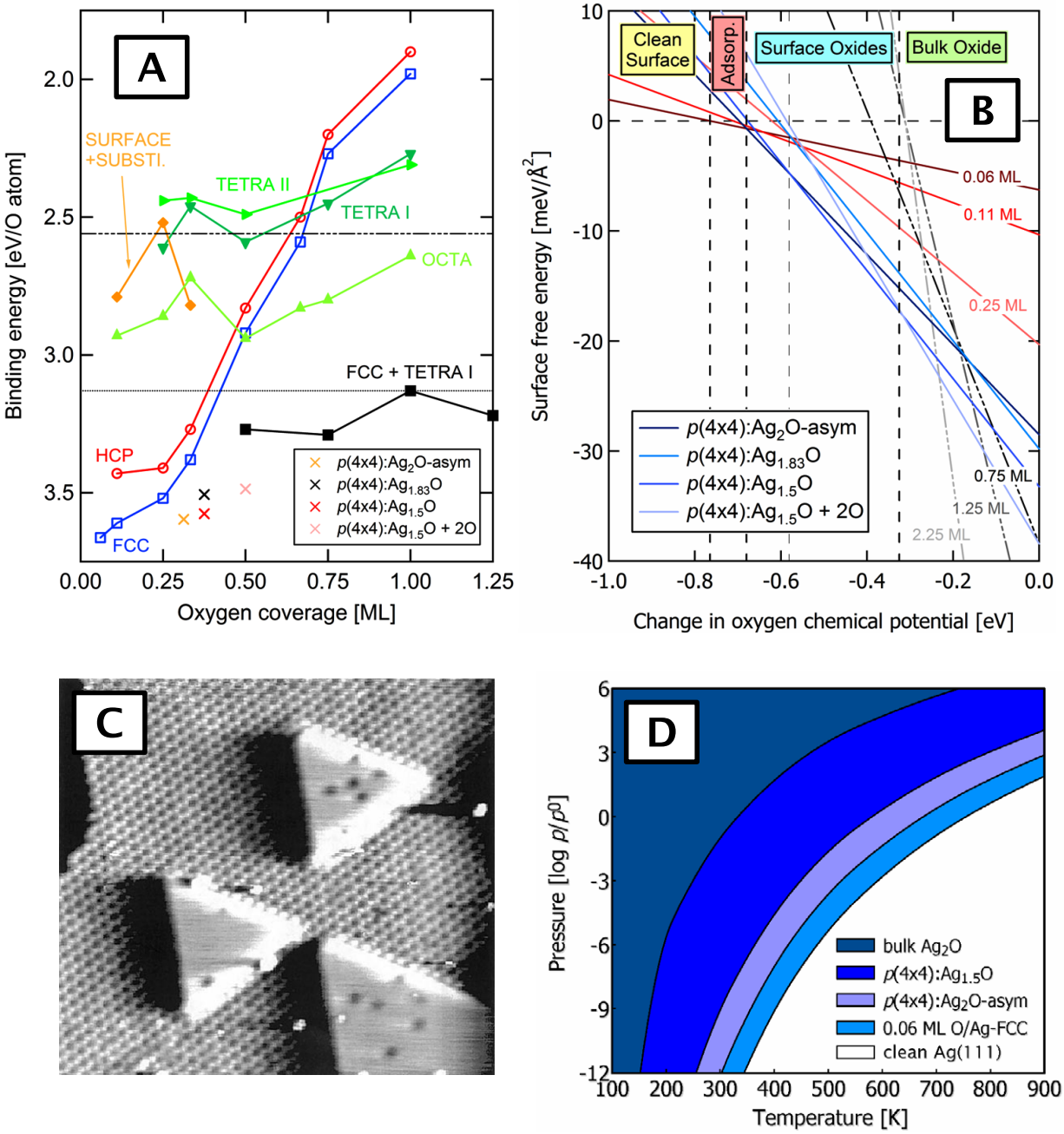

Figure 12. (A) Average binding energies for the O/Ag(111) system (with respect to the free O atom) versus coverage for various structures. The notation for the surface-oxide-like structures is as given in [65]. (Except note that we use the label '$Ag_{1.5}O$' instead of '$Ag_{1.33}O$' to reflect the actual stoichiometry of this structure.) The upper and lower horizontal vertical lines denote the experimental and theoretical values of half the O_2 binding energy, respectively. (B) Surface free energies for various low energy structures as a function of the O chemical potential (given with respect to half the total energy of the O_2 molecule). At the top of the figure, the stable structure types in the corresponding range of chemical potential are listed. (C) STM image of Ag(111) triangular islands within the Ag(111)–$p(4 \times 4)$-O phase. Reprinted from [86]. Copyright 2001 with permission from Elsevier. (D) Calculated (p, T) phase diagram showing the stable structures. (Theoretical results adapted from [65] and [66].)

surface oxides on Au(111) [106], as well as the usual on-surface and subsurface sites, and structures involving both on-surface+subsurface species. The average binding energies of O on Au(111) are summarized in figure 13. As for the other fcc TMs, the fcc site is favored for on-surface adsorption at all coverages. The binding energy significantly decreases for coverages greater than 0.25 ML. At coverage 0.25 ML, the binding energy is less than that of O/Ag(111) (compare ~3.25 eV with ~3.6 eV). The pure subsurface sites are only metastable with respect to free O_2. What is quite striking is that surface-oxide-like structures are significantly more favorable than on-surface adsorption, even for on-surface adsorption at the lowest coverages considered.

Once again, to correlate the effects of temperature and pressure via the change in the oxygen chemical potential, we plot the change in the Gibbs free surface energy of adsorption

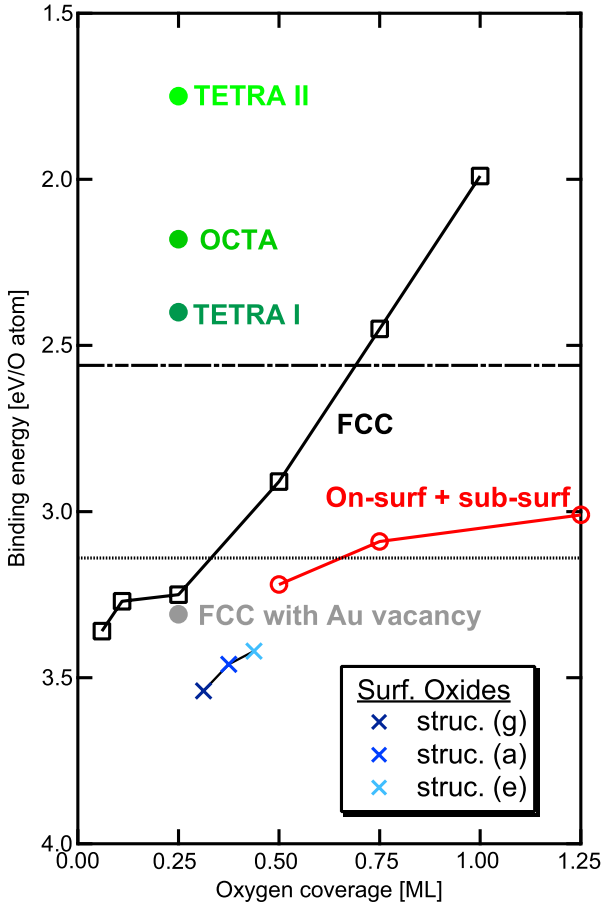

Figure 13. Average binding energy of oxygen on Au(111) (with respect to the free O atom) for homogeneous chemisorption phases with O in the favorable fcc site, the three subsurface sites for 0.25 ML, and the energetically most favorable surface oxides as a function of oxygen coverage. (Note: 'struc.(g)' corresponds to that labeled '$p4$-OCu_3' for O/Cu(111), which is the same as that labeled 'Ag_2O-asym' for O/Ag(111). 'Struc.(a)' corresponds to that labeled 'p4' for O/Cu(111), which is the same as that labeled '$Ag_{1.5}O$' for the O/Ag(111) system. 'Struc.(e)' is the same as that labeled '$p4 + O_F$' for O/Cu(111).) Half the binding energy of O_2, experiment and theory, is indicated by the upper and lower horizontal lines, respectively. (Adapted from [106].)

as a function of the change in the oxygen chemical potential, as presented in figure 14(a). By employing the ideal gas law, we obtain the p–T relations via the oxygen chemical potential and re-map the results in figure 14(a) into a (p, T) phase diagram, shown in figure 14(b). It can be seen that the only stable phases predicted are the thin surface-oxide-like structure (shown in figure 14(c)) for a range of the oxygen chemical potential from -0.17 to -0.4 eV, and the bulk oxide (but only marginally for $T < 100$ K, not shown). The (p, T) range in which the surface-oxide-like structure is predicted to be stable is e.g. 200–420 K at a pressure of 1 atm. We note that it is of course possible that lower energy structures exist that we have not considered, so the energy of this configuration should be taken as an upper limit, and more realistic structures would be even more stable. The finding that such surface oxide structure is predicted to be stable under conditions at which low temperature gold-based catalysts are active raises the question of whether such atomic configurations could play a role in the high catalytic activity of gold nanoparticles. Indeed, to further understand the 'mysterious' nature of the O/Au(111) system calls for further experimental investigations under controlled conditions, that could possibly identify such thin surface-oxide-like structures.

4.4. The oxygen–Cu–Ag (111) system

The use of bimetallic catalysts has been the focus of much work in the field of heterogeneous catalysis [107], since the catalytic activity and selectivity of a metal can be modified substantially by alloying with another metal. For example, new geometrical and electronic effects obtained by varying the alloy composition may play a crucial role in determining the properties of the catalyst [108] and hence open the possibility of rationally designing the catalytic behavior of the material.

Recently, interesting results for an Ag–Cu alloy have been reported, on the basis of both first-principles calculations [109] and experiments [110]. Namely, if instead of pure Ag an Ag–Cu alloy is used as a catalyst for ethylene epoxidation, the selectivity toward ethylene oxide will be improved. Through *ex situ* x-ray photoelectron spectroscopy (XPS) measurements of Ag–Cu systems, it has been shown that the copper surface content is much higher than the overall copper content of the alloy [109, 110], therefore suggesting copper segregation to the surface. This led Linic *et al* [62, 64] to theoretically model the surface of the Ag–Cu alloy assuming a perfect Ag(111) surface in which one out of four silver atoms is replaced by a copper atom. However, it is known that copper, at the temperature T and pressure p_{O_2} used in such experiments ($T = 528$ K, $p_{O_2} = 0.1$ atm), oxidizes to CuO [111], while at higher temperature or lower pressure Cu_2O is the stable oxide [111]. Thus, it is possible that more complex structures involving copper oxides are present on the catalyst surface.

Using DFT we have recently investigated this possibility [112]. Our calculations were performed using the PWscf code contained in the Quantum-ESPRESSO package [113] with the generalized gradient approximation (GGA) of Perdew–Burke–Ernzerhof (PBE) [84] for the exchange and correlation functional, and ultrasoft pseudopotentials [114, 115]. The surface energy of Ag(111) is calculated to be $\gamma^{Ag(111)} = 0.047$ eV Å^{-2} (exp. [116] 0.078 eV Å^{-2}): much smaller than that of Cu(111), $\gamma^{Cu(111)} = 0.076$ eV Å^{-2} (exp. [117] 0.114 eV Å^{-2}). This suggests that when copper impurities are introduced in silver, it is unlikely for copper to be exposed on the surface. Accordingly, we find that increasing the content of Cu in the first layer of the slab leads to an increase of the surface energy. This is shown in figure 15 as the curve with black dots. The positive slope of the curve indicates that it is unfavorable for Cu atoms migrate to the surface with respect to staying under the surface or in the bulk [118].

When oxygen is adsorbed on the surface, on the other hand, the picture is quite different: the presence of oxygen chemisorbed on the alloy surface has the remarkable effect of reversing the slope of the curve for the surface energy versus Cu surface composition. This can be seen in figure 15, comparing the black dot curve (no oxygen present) with the curve with triangles (full monolayer of oxygen). We find

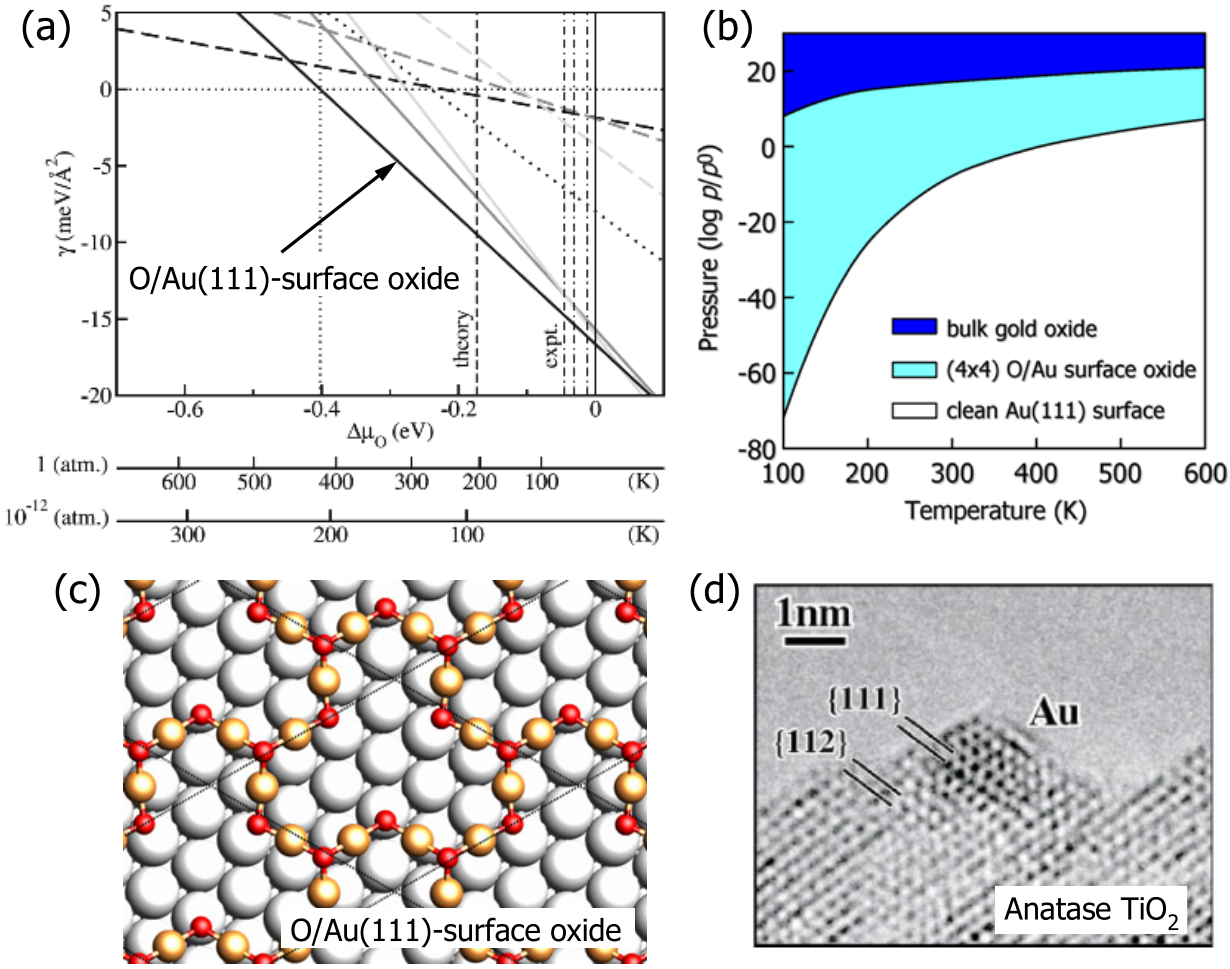

Figure 14. (a) Calculated Gibbs free energy of adsorption (relative to clean Au(111) surface) of low energy structures as a function of oxygen chemical potential, $\Delta\mu_O$ (given with respect to half the total energy of the O_2 molecule). (b) The stability range of the most stable structures evaluated in (a), plotted in (p, T)-space. (c) The atomic geometry of the most favorable surface-oxide-like structure considered. This configuration is the same as that labeled '$p4$-OCu_3' for O/Cu(111) and that labeled 'Ag_2O-asym' for the O/Ag(111) system. The (4×4) surface unit cell is indicated. The oxygen atoms are represented by small dark (red) spheres, the uppermost Au atoms by larger light gray (gold) spheres, and the intact plane of Au(111) atoms lying below is represented by large pale gray spheres. (d) Transmission electron micrograph (TEM) for Au/TiO_2, which clearly shows the exposed {111} microfacet [68]. (Theoretical results are adapted from [106].)

that the presence of a quarter of a monolayer of oxygen is sufficient to invert the slope. The driving mechanism here is the strong affinity between oxygen and copper, which more than compensates the unfavorable surface energy of Cu with respect to Ag: the adsorption energies of oxygen (at 0.25 ML coverage) on Ag(111) and Cu(111) are 0.38 eV/atom and 1.57 eV/atom, respectively. This result agrees with what has been reported in the literature [119].

Since oxygen induces copper segregation to the surface, we now investigate the stability of various surface structures with different contents of copper and oxygen in the first layer. These structures, formed on top of a pure silver slab, are periodic, and the largest surface unit cell employed is the (4×4). We consider three types of structures: (i) chemisorbed oxygen on the Ag–Cu alloy formed in the first layer of the Ag slab, (ii) structures derived from copper(I) oxide Cu_2O, whose structure can be visualized as trilayers of O–Cu–O piled up on top of each other, and (iii) structures derived from copper(II) oxide CuO. We label the first set of chemisorbed structures OxML/CuyML, where x and y are the contents of O and Cu, expressed in monolayers with respect to the underlying Ag(111) surface. Oxygen is adsorbed in the fcc hollow site and copper substitutes silver in the first layer.

For the second set of (Cu_2O-like) structures, we use the label '$p2$' or '$p4$' depending on whether the periodicity of the structure is (2×2) or (4×4) with respect to the clean Ag surface. The '$p4$-OCu_3' configuration is a $p2$ structure (see figure 16(a)) in a (4×4) surface unit cell in which an OCu_3 unit has been removed (see figure 16(b)). (Note that this is a different structure to that considered for the O/Cu(111) system). We also consider thicker films of Cu_2O (up to five atomic layers) in order to extrapolate the behavior of bulk Cu_2O. As we will show in the next section, the two most relevant thin oxide-like structures are '$p2$' and '$p4$-OCu_3'. For this configuration, the average binding energy per oxygen atom is 1.41 eV and 1.37 eV, respectively. For comparison, in bulk Cu_2O the computed formation energy per oxygen atom is 1.26 eV (experimental value 1.75 eV [120]).

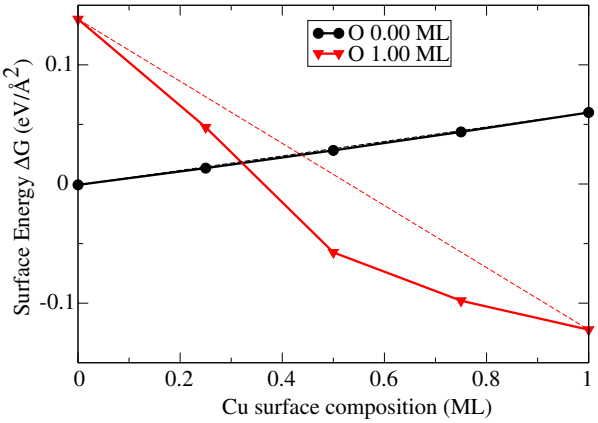

Figure 15. Change in surface free energy (at $T = 0$ K) as a function of Cu concentration in the first layer of Ag(111) for the case of no oxygen present (circles) and for 1 ML of adsorbed oxygen (triangles). The energy zero corresponds to the surface energy of the clean Ag(111) surface. The straight dashed lines are obtained by joining the points corresponding to pure Ag and pure Cu in the first layer. (Adapted from [112].)

For the third set of structures, we consider thin layers of CuO-like structures in a (2 × 2) cell. The one-layer CuO structure (labeled 'CuO(1L)', shown in figure 16(c)) is one of the most favorable, where the binding energy per oxygen atom is 1.16 eV. Thicker films (up to five atomic layers) were also considered in order to extrapolate the behavior of bulk CuO. In this case we must bear in mind that bulk CuO is poorly described with DFT-PBE: CuO is a strongly correlated antiferromagnetic semiconductor, with a monoclinic structure ($a = 4.65$ Å, $b = 3.41$ Å, $c = 5.11$ Å, $\beta = 99.5°$) [121]. DFT-PBE, on the other hand, predicts CuO to be a metal with an almost orthorhombic structure ($a = 4.34$ Å, $b = 4.01$ Å, $c = 5.22$ Å, $\beta = 92.2°$). The predictions for thick films of CuO must therefore be regarded as qualitative. The computed formation energy per oxygen atom in bulk CuO is 1.23 eV (experimental value 1.63 eV [120]).

Considering now all the surface structures mentioned above, and exploiting the vast literature available for the O/Ag system (e.g. [65, 94]) to include the most stable structures for the system in the absence of copper, from the associated surface free energies we are able to construct a phase diagram as a function of the oxygen chemical potential and the copper surface content [112]. This is shown in figure 17. The convex hull, for high Cu content, always includes the structure with the largest number of CuO layers (or Cu_2O layers at lower oxygen chemical potential); i.e., bulk oxide formation is favored beyond a certain Cu surface content. We therefore cut the plot in figure 17 at a Cu composition of 1.50 ML, where it is understood that the rightmost structure is a 'bulk' oxide. However, care must be taken in the meaning given to such 'bulk' structure in the context of a finite system such as the one we are modeling here. We interpret the numerical evidence of the presence of the bulk structure in the convex hull as a tendency for the formation of thick patches of either CuO or Cu_2O.

In the phase diagram shown in figure 17 we have explicitly written the two structures coexisting in a number of regions around the values of interest of oxygen chemical potential and copper content. The labels '$Ag_{1.5}O$' and '$Ag_{1.2}O^{Asym}$' refer to O/Ag structures identified in [65]. If we focus on the region around the chemical potential of interest in typical industrial applications ($\Delta\mu_O \sim -0.6$ eV) and for contents of copper below half a monolayer (consistent with experimental estimations), we predict patches of one-layer oxidic structures ($p4$-Cu_3O) to coexist with the clean Ag surface. At higher values of oxygen chemical potential, on the other hand, O/Ag structures can be found in coexistence with the '$p4$-Cu_3O' structure. At higher Cu contents the '$p2$' and 'CuO(1L)' structures become stable, while for Cu contents beyond one monolayer, bulk CuO is predicted to form. These results suggest that the simple structure adopted in [109] for the Ag–Cu surface alloy to model theoretically the ethylene epoxidation reaction is not stable. Our results, on the other hand, suggest that a model that includes, depending on the Cu surface content, clean Ag(111), patches of oxide-like thin layers and thick layers of CuO, is a more appropriate model for the Ag–Cu catalyst (111) surface.

5. Summary and conclusions

From the consideration and review of the interaction of atomic oxygen with the hexagonal close-packed basal plane of late transition (Ru, Rh, Ir, and Pd) and noble (Cu, Ag, Au) metals, the rich variety of structures that can form depending on the oxygen chemical potential, or correspondingly pressure and temperature conditions, has been highlighted. For these systems there are some general similarities as well as differences: in the order of strongest to weakest O–metal bond at coverage 0.25 monolayer (ML) the following behaviors are found.

'Real' transition metals (here we mean those where the d-band is cut by the Fermi level). (i) O/Ru(0001)—chemisorption on the surface, right up to a full monolayer, is predicted. For higher coverages, surface-oxide-like structures become favorable, which, however, have an energy very similar to the heat of formation of the bulk oxide (per O atom). This presumably explains why no thin oxidic structures are thermodynamically stable in the pressure–temperature (p, T) plots, or, to date, have been observed experimentally. (ii) The O/Rh(111) system exhibits a similar behavior, except that the thin surface oxide structures are more favorable than chemisorption on the surface at full ML. Such structures have been observed experimentally, and interestingly the (p, T) phase diagram indicates that they are only metastable. (iii) The O/Ir(111) system behaves similarly to O/Rh(111) in that the thin surface oxide considered (of the same configuration as on O/Rh(111)) is more favorable than chemisorbed O at 1 ML. In contrast, however, the heat of formation of the bulk oxide (per O atom) is considerably more favorable, and indeed even more so than chemisorbed O at 0.5 ML. The (p, T) phase diagram thus predicts that the only thermodynamically stable phases are the on-surface (2 × 2)-O adsorbate structure and the bulk oxide. To date, there have not been quantitative experimental identifications of such surface oxides on Ir(111). (iv) Regarding O/Pd(111),

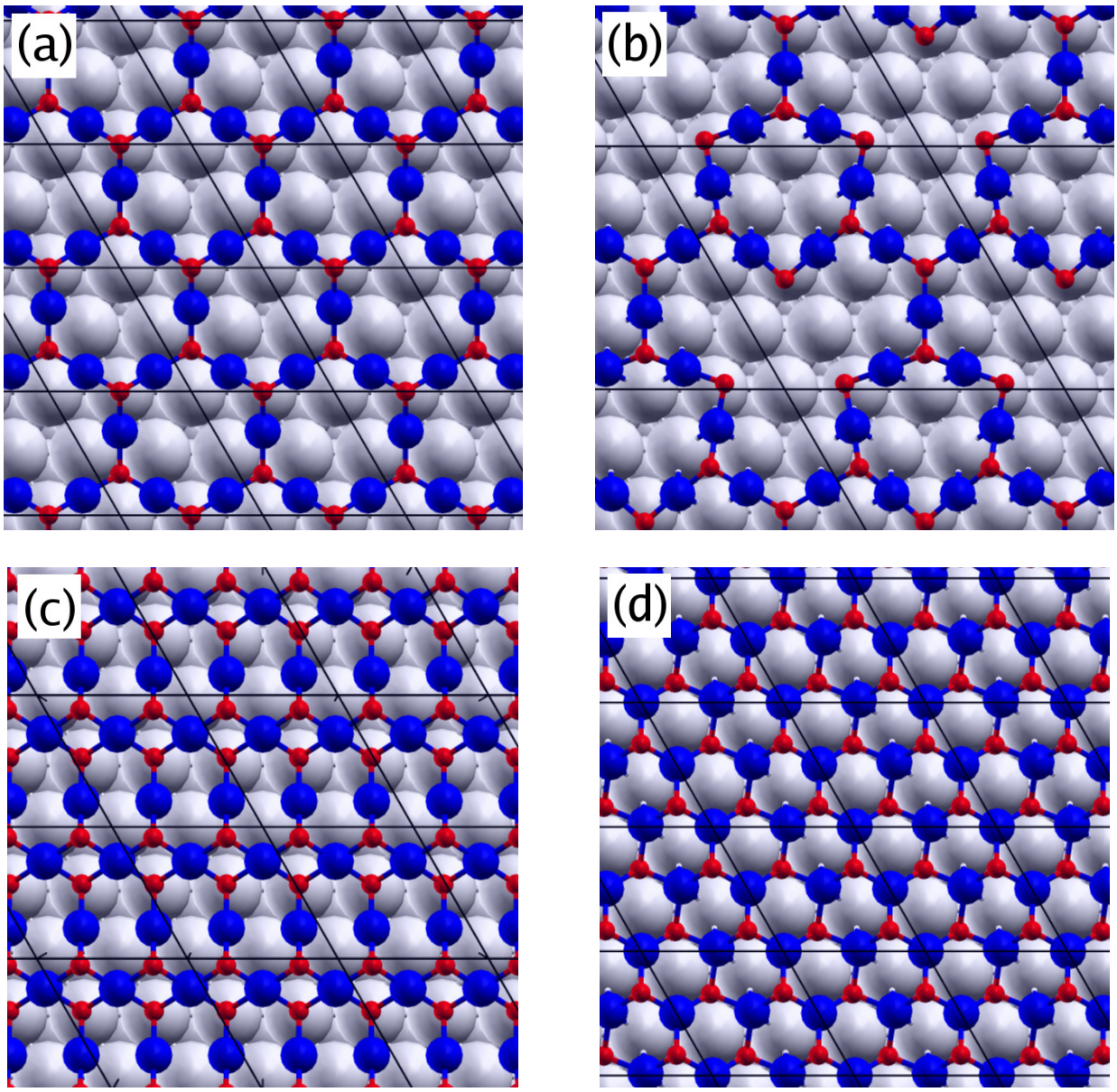

Figure 16. Top view of four of the surface-oxide-like structures considered: (a) '$p2$', (b) '$p4$-OCu_3' (note these two structures are different to those considered for the O/Ag(111) system), (c) 'CuO(1L)' and (d)'O1ML/Cu1ML' (see text). The large pale gray spheres represent the underlying Ag(111) substrate. Surface copper atoms are shown as dark (blue) circles, and oxygen atoms are the small dark (red) circles. The black lines represent the surface unit cells. Reprinted with permission from [112]. Copyright 2008 by the American Physical Society.

this is one of the most investigated and best understood systems. The behavior of this system is somewhat similar to O/Rh(111) in that the surface oxide (which has been experimentally identified) is considerably lower in energy than chemisorption on the surface (here even at 0.5 ML), and also more favorable than the heat of formation of the bulk oxide. Consequently, the free energy phase diagram predicts that both the (2×2)-O adsorption phase, and the surface oxide phase are thermodynamically stable, prior to onset of bulk oxide formation. Recently, experimental and theoretical studies, have shown that a whole host of surface oxidic structures actually form, even though they are apparently only metastable, thus highlighting the complexity of this system.

Noble metals. (v) The O/Cu(111) system exhibits a more extreme behavior than the transition metals mentioned above in that surface-oxide-like structures are more favorable than on-surface adsorption, even at the lowest coverage. They are also notably more stable than the heat of formation of the bulk oxide. The (p, T) phase diagram shows that surface oxides represent thermodynamically stable phases, which form prior to the bulk oxide. Although experimental studies report the existence of such surface oxides, there has been no conclusive determination of the atomic structure. (vi) The O/Ag(111) system is also very well studied, but still bringing surprises, such as the recently reported 'new structure' for the (4×4) phase. The behavior is qualitatively similar to O/Cu(111), except that the absolute stabilities of the various structures

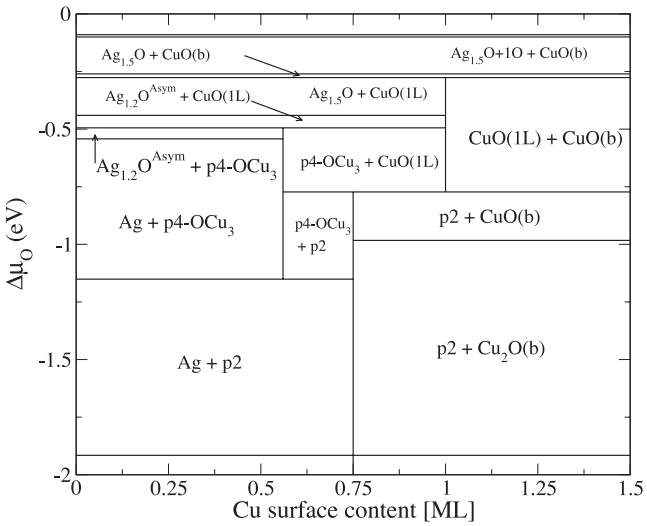

Figure 17. Surface phase diagram showing the structures belonging to the convex hull as a function of the Cu surface content and the change in oxygen chemical potential, $\Delta\mu_O$. The symbol '(b)' indicates bulk structures. The meanings of the labels indicate the (combination of) structures which form in a given region; see the text. Reprinted with permission from [112]. Copyright 2008 by the American Physical Society.

are much reduced. In this case the (p, T) phase diagram predicts that a very low coverage of on-surface oxygen can form ($\leqslant$0.06 ML), followed by surface oxides, then the bulk oxide. Experimental and theoretical studies have shown that many different, but structurally, related oxidic phases can form, all of which have rather similar energies. Thus, this is also a highly complex system. (vii) O/Au(111) behaves similarly to O/Ag(111) except that no on-surface adsorption is predicted, only surface oxides, followed by bulk oxide formation. To date, there have not been any quantitative experimental reports of such thin oxidic structures, though there have been studies of the formation of thicker 'oxide films'.

The systems for which surface oxides are predicted to be stable under pressure and temperature conditions of typical technical catalysis are O/Pd(111) (and possibly O/Pt(111), though this has not been studied in great detail to date), O/Ag(111), and O/Au(111). Also, from our investigations into the interaction of oxygen with an Ag–Cu alloy, we found that it too is a system where surface oxidic structures are predicted under such conditions, for low Cu concentrations. Clearly it should not be concluded, however, that these are the only systems where surface oxide phases may be important, since studies have shown that metastable structures can form as well, due to kinetic stabilization effects.

In the present paper, we have only focused on oxygen at the hexagonal close-packed metal surfaces, and although this is the orientation with the lowest surface energy and could be expected to be predominant on real catalyst particles the adsorption of oxygen can change, or even reverse, the relative stabilities of the various crystallographic orientations, as has been observed in recent studies. In particular, there has also clearly been much work done on the interaction of oxygen with the other low index surfaces, (110) and (100), which was not discussed here, and these systems exhibit just as complex and interesting behaviors.

Over the years much progress has been made with regard to elucidating the nature of O/TM interactions through experimental and theoretical investigations, and there is still much to do in the future—and this includes quantitative studies which also describe the presence of the reactants.

Acknowledgments

We gratefully acknowledge support from the Australian Research Council (ARC), the Australian Partnership for Advanced Computing (APAC) National Facility and the Australian Centre for Advanced Computing and Communications (ac3).

References

[1] Ertl G, Knözinger H and Weitkamp J (ed) 1997 *Handbook of Heterogeneous Catalysis* (New York: Wiley)
[2] Ertl G 2002 *J. Mol. Catal.* A **182** 5
[3] Engel T and Ertl G 1982 Oxidation of carbon monoxide *The Chemical Physics of Solid Surfaces and Heterogeneous Catalysis* ed D A King and D P Woodruff (Amsterdam: Elsevier)
[4] Henrich V E and Cox P A 1993 *The Surface Science of Metal Oxides* (Cambridge: Cambridge University Press)
[5] Fromhold A T 1976 *Theory of Metal Oxidation* vol I & II (Amsterdam: North-Holland)
[6] Besenbacher F and Nørskov J K 1993 *Prog. Surf. Sci.* **44** 5
[7] Campbell C T 2006 *Phys. Rev. Lett.* **96** 066106
[8] Freysoldt C, Rinke P and Scheffler M 2007 *Phys. Rev. Lett.* **99** 086101
[9] Lundgren E, Mikkelsen A, Andersen J N, Kresse G, Schmid M and Varga P 2006 *J. Phys.: Condens. Matter* **18** R 481
[10] van Santen R A and Kuipers H P E E 1987 *Adv. Catal.* **35** 265
[11] Knop-Gericke A, Hävecker M, Schedel-Niedrig T and Schlögl R 2000 *Catal. Lett.* **66** 215
[12] Haruta M 2004 *Gold Bull.* **37** 27
[13] Sabatier P 1920 *La Catalyse en Chimie Organique* (Paris: Berange)
[14] Scheffler M 1987 *Physics of Solid Surfaces* ed J Koukal (Amsterdam: Elsevier)
[15] Scheffler M and Dabrowski J 1988 *Phil. Mag.* A **58** 107
[16] Qian G-X, Martin R and Chadi D J 1998 *Phys. Rev.* B **38** 7649
[17] Wang X-G, Weiss W, Shaikhutdinov Sh K, Ritter M, Petersen M, Wagner F, Schlögl R and Scheffler M 1998 *Phys. Rev. Lett.* **81** 1038
[18] Reuter K and Scheffler M 2002 *Phys. Rev.* B **65** 035406
[19] Łodzianan Z and Nørskov J K 2003 *J. Chem. Phys.* **118** 11179
[20] Kaxiras E, Bar-Yam Y, Joannopoulos J D and Pandy K C 1987 *Phys. Rev.* B **35** 9625
[21] Li W-X, Stampfl C and Scheffler M 2003 *Phys. Rev.* B **67** 045408
[22] Sun Q, Reuter K and Scheffler M 2003 *Phys. Rev.* B **67** 205424
[23] Soon A, Todorova M, Delley B and Stampfl C 2006 *Phys. Rev.* B **73** 165424
[24] Stull D R and Prophet H 1971 *JANAF Thermochemical Tables* 2nd edn (Washington, DC: US National Bureau of Standards)
[25] Van de Walle C G and Neugebauer J 2002 *Phys. Rev. Lett.* **88** 066103

[26] Cant N W, Hicks P C and Lennon B S 1978 *J. Catal.* **54** 372
[27] Peden C H F and Goodman D W 1986 *J. Phys. Chem.* **90** 1360
[28] Madey T E, Engelhardt H A and Menzel D 1975 *Surf. Sci.* **48** 304
[29] Stampfl C, Ganduglia-Pirovano M V, Reuter K and Scheffler M 2002 *Surf. Sci.* **500** 368
[30] Troullier N and Martins J L 1991 *Phys. Rev.* B **43** 1993
[31] Stumpf R and Scheffler M 1994 *Comput. Phys. Commun.* **79** 447
Bockstedte M, Kley A, Neugebauer J and Scheffler M 1997 *Comput. Phys. Commun.* **107** 187
[32] Perdew J P, Chevary J A, Vosko S H, Jackson K A, Pederson M R, Singh D J and Fiolhais C 1992 *Phys. Rev.* B **46** 6671
[33] Stampfl C, Kreuzer H J, Payne S H and Scheffler M 1999 *Appl. Phys.* A **69** 471
[34] Reuter K, Ganduglia-Pirovano M V, Stampfl C and Scheffler M 2002 *Phys. Rev.* B **65** 165403
[35] Stampfl C 2005 *Catal. Today* **105** 17
[36] Stampfl C and Scheffler M 1996 *Phys. Rev.* B **54** 2868
[37] Over H, Kim Y D, Seitsonen A P, Wendt S, Lundgren E, Schmid M, Varga P, Morgante A and Ertl G 2000 *Science* **287** 1474
[38] Ganduglia-Pirovano M V, Scheffler M, Baraldi A, Lizzit S, Comelli G, Paolucci G and Rosei R 2001 *Phys. Rev.* B **63** 205415
[39] Köhler L, Kresse G, Lundgren E, Schmid M, Gustafson J, Mikkelsen A, Borg M, Yuhara J, Andersen J N and Varga P 2004 *Phys. Rev. Lett.* **93** 266103
[40] Gibson K D, Viste M, Sanchez E C and Sibener S J 2000 *J. Chem. Phys.* **112** 2470
[41] Gustafson J, Mikkelsen A, Borg M, Lundgren E, Köhler L, Kresse G, Schmid M, Varga P, Yuhara J, Torrelles X, Quiros C and Andersen J N 2004 *Phys. Rev. Lett.* **92** 126102
[42] Ganduglia-Pirovano M V, Reuter K and Scheffler M 2002 *Phys. Rev.* B **65** 245426
[43] Kresse G and Hafner J 1993 *Phys. Rev.* B **47** 558
Kresse G and Hafner J 1994 *Phys. Rev.* **49** 14251
Kresse G and Furthmüller J 1996 *Comput. Mater. Sci.* **6** 15
Kresse G and Furthmüller J 1996 *Phys. Rev.* B **54** 11169
Kresse G and Joubert D 1999 *Phys. Rev.* B **59** 1758
[44] Chen W, Ermanoski I and Madey T E 2005 *J. Am. Chem. Soc.* **127** 5014
[45] Wögerbauer C, Maciejewski M and Baiker A 2001 *J. Appl. Catal.* B **34** 11
[46] Chan C M and Weinberg W H 1979 *J. Chem. Phys.* **71** 2788
[47] Conrad H, Kuppers J, Notschke F and Plagge A 1977 *Surf. Sci.* **69** 668
[48] Zhdan P A, Boreskov G K, Boronin A I, Egelhoff W F and Weinberg W H 1976 *Surf. Sci.* **61** 25
[49] Marinova T S and Kostov K L 1987 *Surf. Sci.* **185** 203
[50] Davis J E, Nolan P D, Karseboom S G and Mullins C B 1997 *J. Chem. Phys.* **107** 943
[51] Xu Y and Mavrikakisa M 2002 *J. Chem. Phys.* **116** 10846
[52] Zhang H, Soon A, Delley B and Stampfl C unpublished
[53] Klikovits J, Napetschnig E, Schmid M, Seriani N, Dubay O, Kresse G and Varga P 2007 *Phys. Rev.* B **76** 045405
[54] Lundgren E, Kresse G, Klein C, Borg M, Andersen J N, De Santis M, Gauthier Y, Konvicka C, Schmid M and Varga P 2002 *Phys. Rev. Lett.* **88** 246103
[55] Todorova M, Reuter K and Scheffler M 2004 *J. Phys. Chem.* B **108** 14477
[56] Todorova M, Reuter K and Scheffler M 2005 *Phys. Rev.* B **71** 195403
[57] Shumbera R B, Kan H H and Weaver J F 2007 *Surf. Sci.* **601** 235
[58] Seriani N, Pompe W and Ciacchi L C 2006 *J. Phys. Chem.* B **110** 14860
[59] Zhou L, Günther S, Moszynski D and Imbihl R 2005 *J. Catal.* **235** 359
[60] Huang T-J and Tsai D-H 2003 *Catal. Lett.* **87** 173
[61] Rozovskii A Y and Lin G I 2003 *Top. Catal.* **22** 137
[62] Linic S and Barteau M A 2002 *J. Am. Chem. Soc.* **124** 310
[63] Linic S and Barteau M A 2003 *J. Catal.* **214** 200
[64] Linic S and Barteau M A 2003 *J. Am. Chem. Soc.* **125** 4034
[65] Michaelides A, Reuter K and Scheffler M 2005 *J. Vac. Sci. Technol.* A **23** 1487
[66] Li W-X, Stampfl C and Scheffler M 2003 *Phys. Rev. Lett.* **90** 256102
[67] Haruta M, Yamada N, Kobayashi T and Iijima S 1998 *J. Catal.* **115** 301
[68] Haruta M 2003 *Chem. Rec.* **3** 75
[69] Xu Y and Mavrikakis M 2001 *Surf. Sci.* **494** 131
[70] Torres D, Neyman K M and Illas F 2006 *Chem. Phys. Lett.* **429** 86
[71] Matsumoto T, Bennett R A, Stone P, Yamada T, Domen K and Bowker M 2001 *Surf. Sci.* **471** 225
[72] Spitzer A and Luth H 1982 *Surf. Sci.* **118** 136
[73] Judd R W, Hollins P and Pritchard J 1986 *Surf. Sci.* **171** 643
[74] Rajumon M K, Prabhakaran K and Rao C N R 1990 *Surf. Sci.* **233** L237
[75] Niehus H 1983 *Surf. Sci.* **130** 41
[76] Haase J and Kuhr H-J 1998 *Surf. Sci.* **203** L695
[77] Luo B and Urban J 1991 *J. Phys.: Condens. Matter* **3** 2873
[78] Toomes R L, Woodruff D P, Polcik M, Bao S, Hofmann P and Schindler K M 2000 *Surf. Sci.* **443** 300
[79] Jensen F, Besenbacher F, Lægsgaard E and Stensgaard I 1991 *Surf. Sci.* **259** L774
[80] Johnston S M, Mulligan A, Dhanak V and Kadodwala M 2002 *Surf. Sci.* **519** 57
[81] Ertl G 1967 *Surf. Sci.* **6** 208
[82] Wiame F, Maurice V and Marcus P 2007 *Surf. Sci.* **601** 1193
[83] Delley B 1990 *J. Chem. Phys.* **92** 508
Delley B 2000 *J. Chem. Phys.* **113** 7756
[84] Perdew J P, Burke K and Ernzerhof M 1996 *Phys. Rev. Lett.* **77** 3865
[85] Schumacher N, Boisen A, Dahl S, Gokhale A A, Kandoi S, Grabow L C, Dumesic J A, Mavrikakis M and Chorkendorff I 2005 *J. Catal.* **299** 265
[86] Carlisle C I, Fujimoto T, Sim W S and King D A 2000 *Surf. Sci.* **470** 15
[87] Bocquet M-L, Michaelides A, Loffreda D, Sautet P, Alavi A and King D A 2003 *J. Am. Chem. Soc.* **125** 5620
[88] Bocquet M-L, Michaelides A, Sautet P and King D A 2003 *Phys. Rev.* B **68** 075413
[89] Michaelides A, Bocquet M-L, Sautet P, Alavi A and King D A 2002 *Chem. Phys. Lett.* **367** 344
[90] Li W X, Stampfl C and Scheffler M 2002 *Phys. Rev.* B **65** 075407
[91] Li W X, Stampfl C and Scheffler M 2003 *Phys. Rev.* B **67** 045408
[92] Li W X, Stampfl C and Scheffler M 2003 *Phys. Rev.* B **68** 165412
[93] Schmid M, Reicho A, Stierle A, Costina I, Klikovits J, Kostelnik P, Dubay O, Kresse G, Gustafson J, Lundgren E, Andersen J N, Dosch H and Varga P 2006 *Phys. Rev. Lett.* **96** 146102
[94] Schnadt J, Michaelides A, Knudsen J, Vang R T, Reuter K, Lægsgaard E, Scheffler M and Besenbacher F 2006 *Phys. Rev. Lett.* **96** 146101
[95] Czanderna W 1977 *J. Vac. Sci. Technol.* **14** 408
[96] Campbell C T 1985 *Surf. Sci.* **157** 43
[97] Meyer R, Lemire C, Shaikhutdinov Sh K and Freund H-J 2004 *Gold Bull.* **37** 72
[98] Boccuzzi F and Chiorino A 2000 *J. Phys. Chem.* B **104** 5414
[99] Boccuzzi F, Chiorino A and Manzoli M 2001 *Mater. Sci. Eng.* C **15** 215

[100] Kim T S, Stiehl J D, Reeves C T, Meyer R J and Mullins C B 2003 *J. Am. Chem. Soc.* **125** 2018
[101] Stiehl J D, Kim T S, Reeves C T, Meyer R J and Mullins C B 2004 *J. Phys. Chem.* B **108** 7917
[102] Molina L M, Rasmussen M D and Hammer B 2004 *J. Chem. Phys.* **120** 7673
[103] Molina L M and Hammer B 2005 *Appl. Catal.* A **291** 21
[104] Mavrikakis M, Stoltze P and Nørskov J K 2000 *Catal. Lett.* **64** 101
[105] Ricci D, Bongiorno A, Pacchioni G and Landman U 2006 *Phys. Rev. Lett.* **97** 036106
[106] Shi H Q and Stampfl C 2007 *Phys. Rev.* B **76** 075327
[107] Sinfelt J H 1983 *Bimetallic Catalysts: Discoveries, Concepts and Application* (New York: Wiley)
[108] Liu P and Nørskov J K 2001 *Phys. Chem. Chem. Phys.* **3** 3814
[109] Linic S, Jankowiak J and Barteau M A 2004 *J. Catal.* **224** 489
[110] Jankowiak J T and Barteau M A 2005 *J. Catal.* **236** 366
[111] Schmidt-Whitley R D, Martinez-Clemente M and Revcolevschi A 1974 *J. Cryst. Growth* **23** 113
[112] Piccinin S, Stampfl C and Scheffler M 2008 *Phys. Rev.* B **77** 075426
[113] Baroni S, Corso A D, de Gironcoli S, Giannozzi P, Cavazzoni C, Ballabio G, Scandolo S, Chiarotti G, Focher P, Pasquarello A, Laasonen K, Trave A, Car R, Marzari N and Kokalj A *Quantum-espresso* http://www.pwscf.org.
[114] Vanderbilt D 1990 *Phys. Rev.* B **41** 7892
[115] The ultrasoft pseudopotential for Ag, Cu and O were taken from the PWscf pseudopotential download page http://www.pwscf.org/pseudo/htm (files: Ag.pbe-d-rrkjus.UPF, Cu.pbe-d-rrkjus.UPF, O.pbe-rrkjus.UPF)
[116] De Boer F R, Boom R, Mattens W C M, Miederna A R and Niessen A K 1988 *Cohesion in Metals* (Amsterdam: North-Holland)
[117] Lindgren S A, Walldén L, Rundgren J and Westrin P 1984 *Phys. Rev.* B **29** 576
[118] Christensen A, Ruban A V, Stoltze P, Jacobsen K W, Skriver H K, Norskov J K and Besenbacher F 1997 *Phys. Rev.* B **56** 5822
[119] Kangas T, Nivalainen N, Pitkänen H, Puisto A, Alatalo M and Laasonen K 2006 *Surf. Sci.* **600** 4103
[120] *CRC Handbook of Chemistry and Physics* 1995 (Boca Raton FL: CRC Press)
[121] Kim J Y, Rodriguez J A, Hanson J C, Frenkel A I and Lee P L 2003 *J. Am. Chem. Soc.* **125** 10684